

EMISSIVITY OF AXIONS FROM HOT NUCLEAR  
MATTER

NOAH KAKEKASPAN

Department of Physics  
McGill University, Montreal, QC  
July 2024

A thesis submitted to McGill University in partial fulfillment of the  
requirements of the degree of Master of Science

© Noah Kakekaspan, 2024



# CONTENTS

---

<b>i</b>	<b>Theoretical Background</b>	
1	Introduction	3
1.1	Quantum Chromodynamics	5
1.2	QCD Phase Diagram	8
2	The Strong CP Problem and $U(1)_{PQ}$ Symmetry	11
2.0.1	Axion Interactions	15
3	Neutron Star Physics	21
3.0.1	Neutron Star Cooling	22
3.0.2	Conditions during Neutron Star Mergers	25
3.0.3	Neutron Star Equation of State	26
<b>ii</b>	<b>Calculating the Axion Emissivity</b>	
4	Emissivity through Bremsstrahlung	35
4.0.1	Kinematics	35
4.0.2	Neutrino Bremsstrahlung Rates	39
4.0.3	Axion Bremsstrahlung Rates	40
<b>iii</b>	<b>Results</b>	
5	Axion Bremsstrahlung Emissivities	49
<b>iv</b>	<b>Conclusion</b>	
6	Conclusion	63
<b>v</b>	<b>Appendix</b>	
A	C++ Code	66
	Bibliography	67

## LIST OF FIGURES

---

- Figure 1.1 The particles of the Standard Model, divided in fermions (quarks and leptons) and bosons (gauge bosons and scalar boson). The different masses, charge (in terms of electron charge  $e$ ), and spin are labelled, and the different fermion generations are distinguished, where higher generations possess larger masses [1]. 4
- Figure 1.2 Observed rotational velocity compared to the expected rotational velocity of M33, a dwarf spiral galaxy, where the rotational velocity is in kilometres per second (km/s) vs the distance in kiloparsecs (kpc) from the center of the galaxy [5]. 5
- Figure 1.3 Strong Coupling  $\alpha_s(Q^2)$  data at discrete energy scales  $Q$ , with  $N_c = 3$  in Eq. 1.9, taken from ref. [2]. The data for  $\alpha_s(Q^2)$  are taken up to next-to-next-to-leading order (NNLO), while Eq. 1.9 is only up to leading order (LO). NNLO corresponds to the three-loop correction to  $\alpha_s$ , whereas LO uses only one-loop Feynman diagram corrections. 8
- Figure 1.4 3-Dimensional QCD phase diagram at high densities and with an isospin asymmetry (refer to Eq. 3.18 for isospin asymmetry term). The phase diagram shows different structures for nuclear matter and the experiments used to probe such structures, with the critical points and phase transitions included [15]. 9
- Figure 2.1 Axion mass and decay constant, based on different astronomical observations and experimental efforts, with preinflation and postinflation PQ breaking scenarios calculated using Lattice topology [29]. 15
- Figure 2.2 Feynman diagrams for nucleon-nucleon-axion bremsstrahlung. There are eight different diagrams to consider, where the couplings to the pion and axion are effective field theory couplings shown in Eq. 2.15 and Eq. 2.16. 18
- Figure 3.1 The layers of a typical neutron star [53]. 22
- Figure 3.2 The energy per nucleon calculated using the FSUGold2 equation of state at different densities and different proton fractions, where  $k_F = (\frac{3}{2}\pi^2 n)^{1/3}$  and is the nucleon density  $n = n_n + n_p$  [65]. 31
- Figure 5.1 Analytical nucleon-nucleon-axion bremsstrahlung emission rates compared to numerical nucleon-nucleon-axion bremsstrahlung emission rates, within  $-4 \leq y \leq 10$  range. The results here are made dimensionless by only plotting the  $y$  dependent terms  $e^{2y}$  and  $y^{1/2}$ , and ignoring the  $f^2 g_{ai}^2 m^{2.5} m_\pi^{-4} T^{6.5}$  portion of the equations for the emissivities. 51

- Figure 5.2 Ratio between effective mass and bare mass, which is  $m_p = 938\text{MeV}$  and  $m_n = 939\text{ MeV}$ , for proton and neutrons. The equation of state is FSUGold2 [65]. 52
- Figure 5.3 Shown is the  $y$ -value for neutrons and protons at increasing densities up to  $10n_0$ , where the temperature is set to  $T = 6\text{ MeV}$ . 54
- Figure 5.4 Neutron-neutron bremsstrahlung emission rates for axions and neutrinos at  $T = 6\text{ MeV}$ . 55
- Figure 5.5 Proton-proton bremsstrahlung emission rates for axions and neutrinos at  $T = 6\text{ MeV}$ . 55
- Figure 5.6 Shown is the  $y$ -value for neutrons and protons at increasing densities, with the temperature set to  $T = 10\text{ MeV}$ . 57
- Figure 5.7 Neutron-neutron bremsstrahlung emission rates for axions and neutrinos at  $T = 10\text{ MeV}$ . 57
- Figure 5.8 Proton-proton bremsstrahlung emission rates for axions and neutrinos at  $T = 10\text{ MeV}$ . 58
- Figure 5.9 Shown is the  $y$ -value for neutrons and protons at increasing densities, for  $T = 50\text{ MeV}$ . 59
- Figure 5.10 Neutron-neutron bremsstrahlung emission rates for axions and neutrinos at  $T = 50\text{ MeV}$ . 59
- Figure 5.11 Proton-proton bremsstrahlung emission rates for axions and neutrinos at  $T = 50\text{ MeV}$ . 60



## ABSTRACT

---

For this thesis, the emissivity of axions from interactions of nucleons, such as neutrons and protons, is investigated. The rate of axions emitted from nucleon-nucleon-axion bremsstrahlung is calculated assuming nuclear matter under extreme conditions, similar to the medium in neutron star mergers, where the density and temperature can be larger than in a single neutron star. The density and temperature play a role in the emissivity of axions from the medium, and the emission rates for the axion are varied using a nuclear equation of state typically used for highly dense nuclear matter. The axion emission can be a mechanism for neutron star cooling, similar to the Urca processes. The axion emission rates are compared to those of the modified Urca process, where neutrinos are emitted from the medium also through nucleon-nucleon pair bremsstrahlung.

## ABSTRACT

---

Pour cette thèse, l'émissivité des axions résultant des interactions entre les nucléons, tels que les neutrons et les protons, est étudiée. La quantité d'axions émise à partir du bremsstrahlung nucléon-nucléon-axion est calculée en supposant une matière nucléaire dans des conditions extrêmes, similaires à celles lors d'une fusion d'étoiles à neutrons, où la densité et la température peuvent être bien supérieures à celles de simples étoiles à neutrons. La densité et la température jouent un rôle dans l'émissivité des axions, donc les taux d'émission pour l'axion sont variés en utilisant une équation d'état nucléaire typiquement utilisée pour la matière nucléaire très dense. L'émission d'axions peut être un mécanisme de refroidissement des étoiles à neutrons, semblable aux processus Urca. Les taux d'émission d'axions sont comparés à ceux du processus d'Urca modifié, où des neutrinos sont également émis du milieu par le bremsstrahlung de paires nucléon-nucléon.

## ACKNOWLEDGMENTS

---

I would like to express my sincere gratitude to my supervisor, Prof. Charles Gale, whose guidance, support, and patience have been invaluable throughout my master's studies. His insightful feedback and encouragement have significantly contributed to completing this work. I would also like to give my many thanks to Melissa Mendes Silva for all the help they provided me with this thesis. The many resources they provided were greatly appreciated.

I also extend my appreciation to Prof. Sangyong Jeon, Roozbeh Yazdi, Matthew Ramin Hamedani, Nicolas Fortier, and Jessica Churchill for their contributions to the development of the code utilized in my thesis. Their expertise and willingness to share knowledge during our group meetings and one-on-one help have been immensely helpful in implementing the necessary tools and techniques for my research objectives.

My friends during my master's also deserve a large acknowledgement since they are the ones who helped me through classwork and also made my time at McGill enjoyable.

Lastly, I would like to thank my family, who I rarely got to see during my time in Montreal. Even when they were 2000 km away, they supported my studies, and knowing they were proud of where I was kept me going.



Part I

THEORETICAL BACKGROUND



## INTRODUCTION

---

Quantum field theories (QFTs) are the language particle physicists use to describe particle interactions involving the extensive list of known particles. Particles are conceptualized not as isolated entities but as excitations of underlying fields that permeate spacetime. Each type of particle is associated with its specific field. QFTs are also used to develop theories with hypothetical particles. The fundamental fields are the building blocks for more exotic particles, and as far as our modern understanding goes, they are listed in what is called the Standard Model of particle physics. So far, the Standard Model consists of six quarks and six leptons, both making up the fermionic matter in our universe. The Standard Model also includes bosons, which are known to be the force carriers; there is the scalar Higgs boson, the photon, the gluon, and the vector Z and W bosons. The particles seen in Fig. 1.1 are a part of our luminous universe, but there are still sectors, possibly unknown, which make up our dark universe.

Even though the Standard Model has been successful in explaining the properties and interactions of known particles, such as the electron's inherent coupling to photons (known as the fine structure constant  $\alpha = 1/137$ )[2], the Standard Model does not account for the parts of the universe known as dark matter and dark energy. The concept of dark matter began in the early 20th century when astronomers noticed problems with astronomical observations. Galaxies were rotating at velocities that implied the presence of much more mass than what could be accounted for by visible matter alone [3][4]. Fig. 1.2 shows this effect by superimposing rotation curve data on top of an image of M33, which is a dwarf spiral galaxy. In the 21st century, the search for dark matter has become one of the most active areas of physics research. Numerous experiments have been designed to detect dark

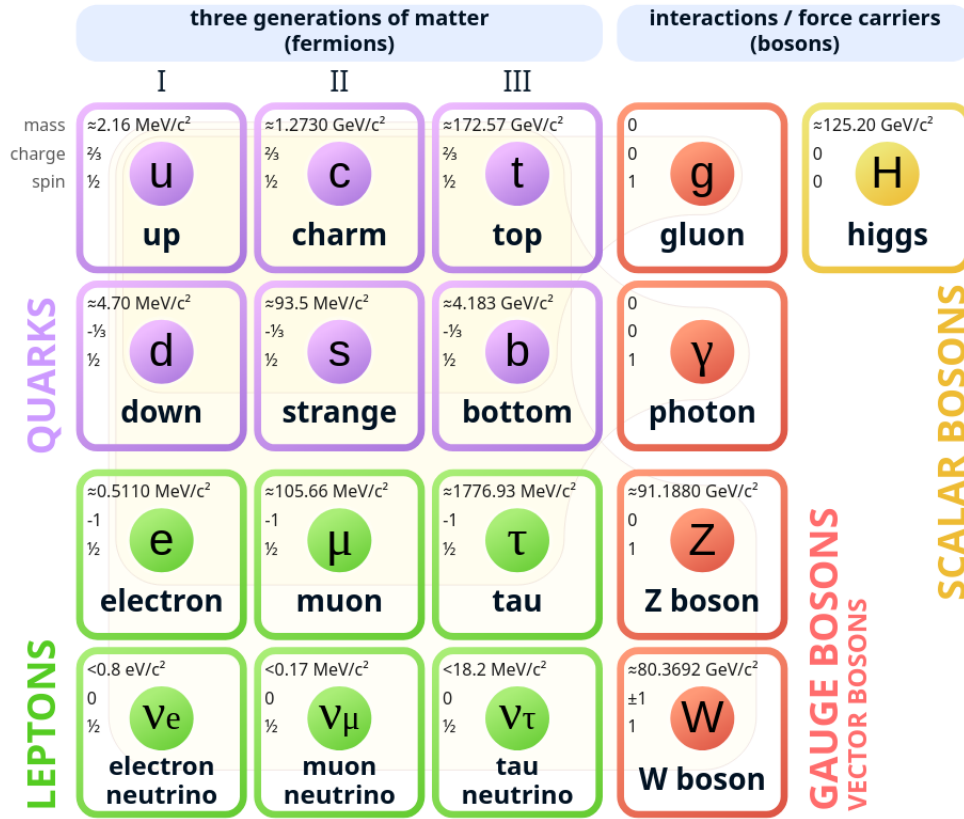


Figure 1.1: The particles of the Standard Model, divided in fermions (quarks and leptons) and bosons (gauge bosons and scalar boson). The different masses, charge (in terms of electron charge  $e$ ), and spin are labelled, and the different fermion generations are distinguished, where higher generations possess larger masses [1].

matter particles directly, such as weakly interacting massive particles (WIMPs) [6], or to observe their effects indirectly through astrophysical observations [7]. The Large Hadron Collider (LHC) and other particle accelerators have also sought signs of dark matter particles in high-energy collisions [8]. Despite these efforts, dark matter remains one of the most elusive components of the universe. Its presence is inferred from gravitational effects on visible matter, radiation, and the universe’s large-scale structure, but its true nature and composition remain unknown.

The purpose of this study is to calculate the emissivity of the Quantum Chromodynamics (QCD) axion, which may be a dark matter candidate, from hot nuclear matter. Emissivity, in the context of axions, refers to the rate at which energy is lost from a medium, such as nuclear matter, as axions are emitted. The search for the axion has significantly contributed to the exploration of viable dark matter. The concept of the axion, alongside axion-like

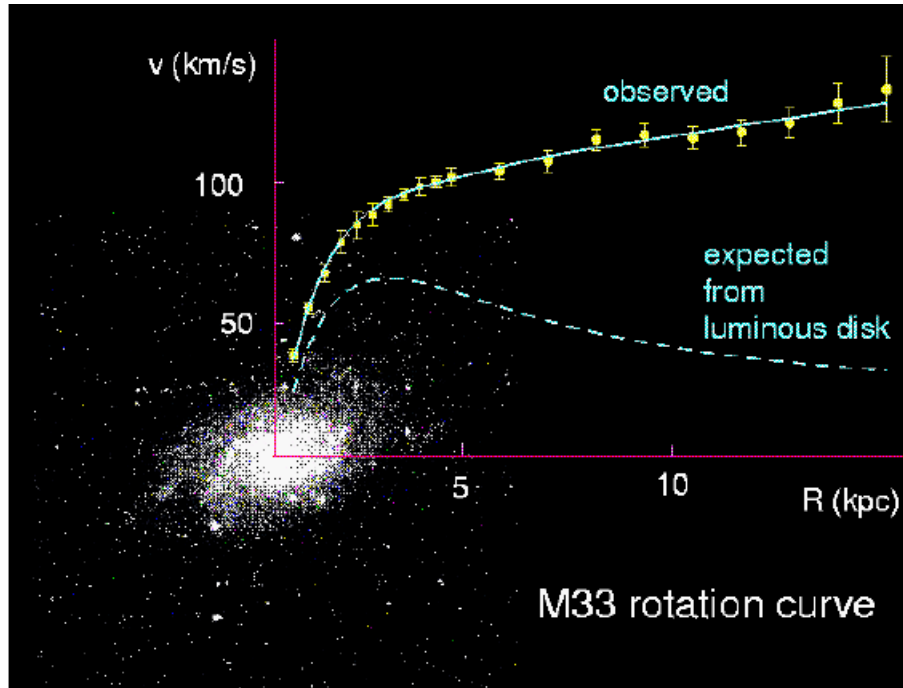


Figure 1.2: Observed rotational velocity compared to the expected rotational velocity of M33, a dwarf spiral galaxy, where the rotational velocity is in kilometres per second (km/s) vs the distance in kiloparsecs (kpc) from the center of the galaxy [5].

particles (ALPs), emerged as a compelling solution to the Strong CP Problem in QCD [9][10][11]. The Strong CP Problem is a theoretical conundrum that questions why CP violation, which is theoretically permissible in the strong force, is not observed in nature. Axions, which are discussed in more detail in section 2, interact very weakly with ordinary matter and radiation, which is a characteristic feature expected of dark matter particles. This weak interaction makes them difficult to detect, similar to other dark matter candidates. The next section will introduce QCD and the QCD phase diagram, which will go over the concepts needed in order to discuss axion interactions and the motivation for why this study will be investigating extreme nuclear conditions.

## 1.1 QUANTUM CHROMODYNAMICS

Gluons are the mediators of the strong nuclear force, binding quarks together through quark-gluon interactions. Without the strong force, the Coulomb repulsion of nuclei in the nucleus

would not allow matter to exist in a stable state. QCD is the field theory that is used to describe the strong nuclear force. The QCD Lagrangian involving quarks and gluons is [12]

$$\mathcal{L}_{QCD} = \bar{\psi} (i\not{\partial} - M - g\not{A}_a G^a) \psi - \frac{1}{4} F_a^{\mu\nu} F_{\mu\nu}^a. \quad (1.1)$$

where  $A_\mu^a$  are the gluon fields,  $a$  is the colour charge index that is equal to  $a = 1, 2, \dots, 8$  for  $SU(3)$ , which is the colour gauge group.  $\psi$  is the quark field for any of the six quark flavours ( $u, d, s, c, t,$  or  $b$  quark flavours),  $M$  is the quark mass, and  $g$  is the coupling constant. The gluon field strength tensor, labelled  $F_a^{\mu\nu}$ , that governs the dynamics of the gluon is defined as

$$F_a^{\mu\nu} = \partial^\mu A_\nu^a - \partial^\nu A_\mu^a + g f^{abc} A_b^\mu A_c^\nu. \quad (1.2)$$

where  $f^{abc}$  is a constant that depends on the colour indices  $a, b,$  and  $c,$  and is antisymmetric between permutations  $f_{abc} = -f_{bac}$ :

$$f_{123} = 1, \quad (1.3)$$

$$f_{147} = -f_{156} = f_{246} = f_{257} = f_{345} = -f_{367} = \frac{1}{2}, \quad (1.4)$$

$$f_{458} = f_{678} = \frac{\sqrt{3}}{2}. \quad (1.5)$$

Like for quantum electrodynamics (QED), the Lagrangian has a kinetic and mass term for describing a non-interacting massive quark. Then, a minimal coupling term for the quarks to the gluons is similar to fermions coupling to photons in QED. Lastly, the invariant term  $F_a^{\mu\nu} F_{\mu\nu}^a$  describes the kinetic energy of the gluons, which has a similar term in the QED Lagrangian for photons. The difference between the two theories is that QED is an abelian theory that uses the  $U(1)$  gauge symmetry, which governs the dynamics of the photon, while QCD is a non-abelian gauge theory with  $SU(3)$  symmetry, which affects the strong force coupling in a non-trivial way. QED is an abelian theory because the group transformations commute [13], and QCD has Lie-group generators from eq. 1.1 that have the cyclic property  $[G^a, G^b] = i f_{abc} G^c$ .

The third term in Eq. 1.2 is not seen in QED, and this gluon self-interacting term causes the non-abelian nature of QCD. The strong coupling, labelled  $g$ , is the strength of interaction between quarks and gluons. Though it is called a constant, it is energy-dependent, where it decays at high energies and is large at low energies. To see the behaviour of  $g$  at different energies, the renormalization of  $g$  up to one loop interactions gives the following beta function [14],

$$\frac{\partial g}{\partial \ln \mu} = \beta(g) = -\left(\frac{11}{3}N_c - \frac{2}{3}n_f\right) \frac{g^3}{(4\pi)^2} + O(g^5). \quad (1.6)$$

Here  $N_c$  is the number of colours, and  $n_f$  is the number of active quark flavours at the scale  $\mu$ . Due to the negative beta function, the QCD field theory experiences a phenomenon known as asymptotic freedom. Asymptotic freedom is a unique feature of QCD, whereby the strong force weakens as the energy scale increases or the distance scale decreases. This behaviour is opposite to the electromagnetic force and is the main behaviour of non-abelian gauge theories like QCD, where gluon self-interactions contribute a negative term to the beta function, contrasting with abelian theories where such self-interactions are absent. It can be convenient to represent the strong coupling in terms of the fine structure constant for the strong interaction, labelled  $\alpha_s$ ,

$$\alpha_s \equiv \frac{g^2}{4\pi} \quad (1.7)$$

$$\frac{\partial \alpha_s}{\partial \ln \mu} = \beta(\alpha_s) = -\left(\frac{11}{3}N_c - \frac{2}{3}n_f\right) \frac{\alpha_s^2}{2\pi} + O(\alpha_s^4) \quad (1.8)$$

Therefore, the renormalized strong coupling can be expressed as

$$\alpha_s(Q^2) = \frac{4\pi N_c}{(11N_c - 2n_f) \ln(Q^2/\Lambda_{QCD}^2)}, \quad (1.9)$$

which varies depending on an arbitrary energy scale  $Q$ , as seen in Fig. 1.3. In the logarithm for  $\alpha_s$  in Eq. 1.9, there is a  $\Lambda_{QCD}$ , which is the scale of the strong interaction and appears as

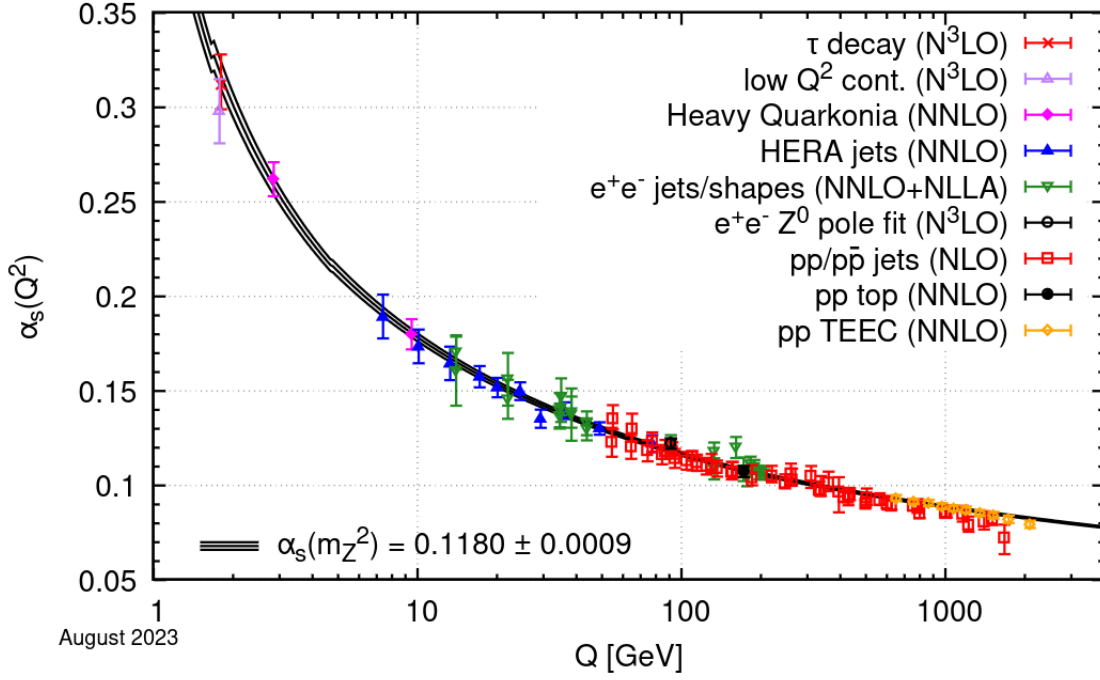


Figure 1.3: Strong Coupling  $\alpha_s(Q^2)$  data at discrete energy scales  $Q$ , with  $N_c = 3$  in Eq. 1.9, taken from ref. [2]. The data for  $\alpha_s(Q^2)$  are taken up to next-to-next-to-leading order (NNLO), while Eq. 1.9 is only up to leading order (LO). NNLO corresponds to the three-loop correction to  $\alpha_s$ , whereas LO uses only one-loop Feynman diagram corrections.

an arbitrary energy scale from the renormalization process. However, the value of  $\Lambda_{QCD}$  is typically chosen to be  $\Lambda_{QCD} \sim 200$  MeV [12].

## 1.2 QCD PHASE DIAGRAM

The QCD phase diagram describes the different possible states of strongly interacting matter, depending on the temperature and density. Fig. 1.4 shows the mostly conjectured QCD phase diagram and the different states of matter. Hadronic matter consists of baryons and mesons, where a baryon has three constituent quarks, and a meson has a constituent quark and anti-quark, which are all held together by gluons. The hadronic matter comprises the diagram's low temperature and low-density region. As the energy is increased, the quarks inside of the hadrons reach a deconfinement transition, resulting in a state of matter called the quark-gluon plasma (QGP), which is thought to exist in the early universe just after the Big Bang. A critical point is theorized to occur which would represent that location

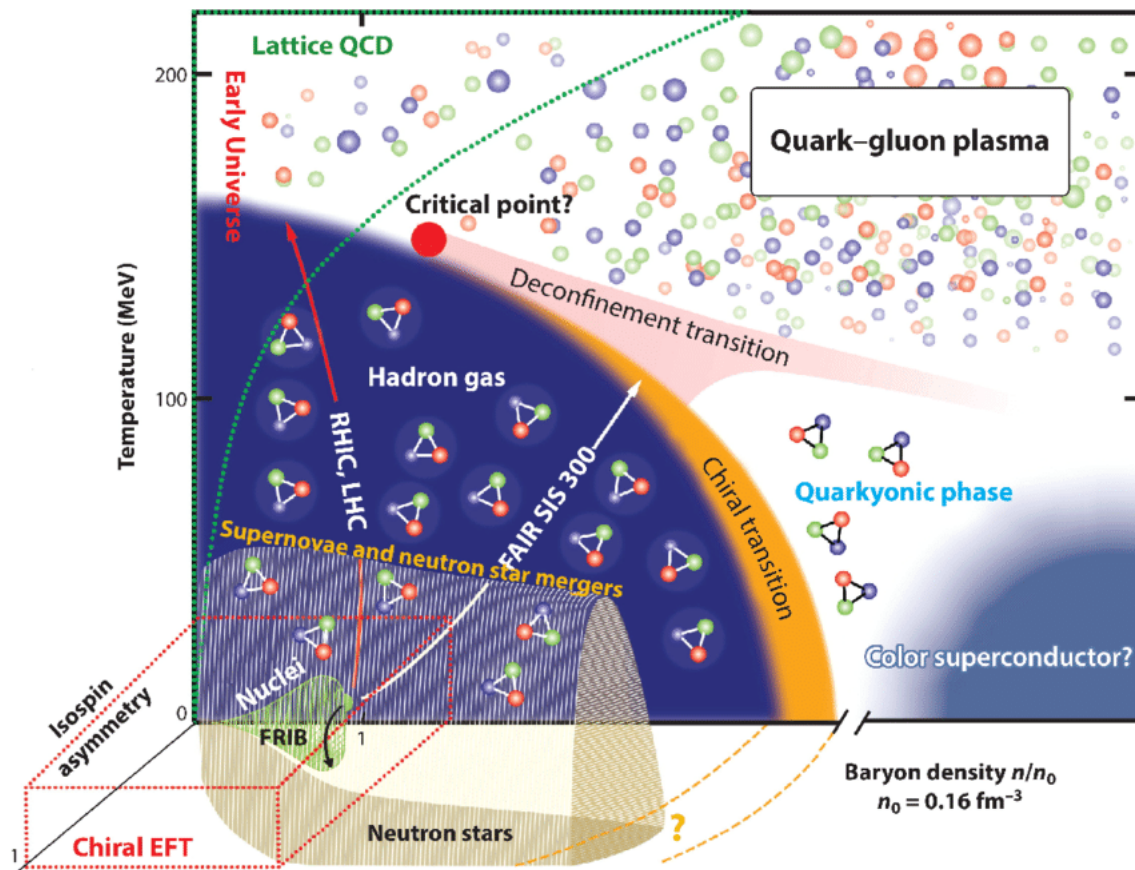


Figure 1.4: 3-Dimensional QCD phase diagram at high densities and with an isospin asymmetry (refer to Eq. 3.18 for isospin asymmetry term). The phase diagram shows different structures for nuclear matter and the experiments used to probe such structures, with the critical points and phase transitions included [15].

in the phase space where hadrons and the QGP both exist. Different laboratories currently probe the nuclear medium in different regions to describe the properties of the strong interaction at these conditions. For the QGP, heavy-ion collision experiments done at LHC and RHIC are done to compare to theory, such as perturbative calculations and lattice QCD. The theorized quarkyonic phase is expected at high density but below the deconfinement temperatures seen in QCD conditions. The quarkyonic phase still contains confined quarks but is past the chiral transition where the quarks are approximated to be massless [16][17]. Past this point at extremely high densities, quarks are hypothesized to experience colour superconductivity: a state in which quarks pair up into Cooper pairs (the attractive force between quarks is mediated by gluons), moving beyond their usual confinement within hadrons [18][19]. Along the low-temperature, high-density axis, astrophysical laboratories

are used since these conditions are produced within the medium of a neutron star. A neutron star experiences a high isospin asymmetry, meaning there are more neutrons compared to protons. The underlying physics within the asymmetry alongside highly dense matter, like within a neutron star, is of interest within this thesis since it can help uncover more meaning to the QCD phase diagram at an isospin density imbalance. This isospin asymmetry will be discussed more in section 3.0.3. Finally, understanding how nucleons interact with particles like the axion is of interest for this study at high densities and at isospin asymmetries. The axion will be introduced in the next chapter.

## THE STRONG CP PROBLEM AND $U(1)_{PQ}$ SYMMETRY

---

For any field, we can translate the field in the spatial direction  $\vec{x}$  and perform rotations around an axis. A parity transformation geometrically shifts the position by  $\vec{x} \rightarrow -\vec{x}$ . Charge conjugate flips the electric charge of the field, and does not affect neutral charges. Charge conjugation (C) and parity (P) together is so far known to not be violated for strong interactions, meaning observations in experiments have not found a process that violates CP symmetry [20].

In QCD, the consequence of the gluon topology allows the infinite number of degenerate vacuum states known as the  $\theta$ -vacua [21]. These vacuum states emerge due to solutions to the Yang-Mills equations called instantons [22]. Instantons can be described as pseudoparticles that are characterized by a quantized topological charge known as the winding number. Each instanton solution contributes to the tunnelling between different  $\theta$ -vacuum states characterized by different winding numbers,  $|n\rangle$  [23]. These vacuum states take the form

$$|\theta\rangle = \frac{1}{\sqrt{2\pi}} \sum_n e^{-in\theta} |n\rangle, \quad (2.1)$$

where  $n$  is the winding number, which is an integer, and  $\theta$  can take any value between  $[-\pi, \pi]$ . These states introduce a term in the QCD Lagrangian that is CP-violating,

$$\mathcal{L}_\theta = \bar{\theta} \frac{g^2}{32\pi^2} F_a^{\mu\nu} \tilde{F}_{a\mu\nu}, \quad \text{with} \quad \bar{\theta} = \theta + \text{argdet}(M). \quad (2.2)$$

This term includes the gluon tensor  $F_a^{\mu\nu}$ , the dual gluon tensor  $\tilde{F}_{a\mu\nu} = \frac{1}{2} \epsilon_{\mu\nu\alpha\beta} F_a^{\alpha\beta}$ , the strong coupling  $g$ , and  $\bar{\theta}$ . The  $\text{argdet}(M)$  term is the complex polar angle of  $\det(M)$ , where  $M$  is the mass matrix for quarks. The CP-violation occurs since the Levi-Civita tensor  $\epsilon_{\mu\nu\alpha\beta}$  changes

sign after a parity transformation due to the odd number of spacial components, while  $F_a^{\mu\nu}$  is invariant under CP. Therefore, after a CP transformation  $\tilde{F}_{a\mu\nu} \rightarrow -\tilde{F}_{a\mu\nu}$ , resulting in the  $\mathcal{L}_\theta$  term in the QCD Lagrangian to violate CP symmetry. Even though it is theoretically allowed to violate CP, there is no evidence of CP violation for strong interactions. To investigate experimentally, the  $\mathcal{L}_\theta$  term can be shown to contribute to the quark's electric dipole moment (EDM), and in turn the neutron's EDM,  $d_n$  [13]. From deriving the theoretical estimate for  $d_n$ , the expression is [24]

$$d_n \sim e\bar{\theta}\frac{m_q}{m_n^2} \approx 2.4 \times 10^{-16}\bar{\theta} e \cdot \text{cm}. \quad (2.3)$$

Experimental bounds on  $d_n$  are about  $|d_n| \leq 2.9 \times 10^{-26} e \cdot \text{cm}$  [25], which gives upper limit to the magnitude of  $\bar{\theta}$  to equal  $|\bar{\theta}| \leq 10^{-10}$ . The magnitude of  $\bar{\theta}$  can range from  $[0, \pi)$ , making it notable that its observed value is close to zero. Given that  $\bar{\theta} \approx 0$ , no CP-violation has yet been detected in strong interactions. This situation, where theoretical expectations allow for a potentially larger value but observations suggest a near-zero value, is known as the Strong CP Problem, and is suggestive of an underlying symmetry.

Several solutions have been proposed to resolve the Strong CP Problem. In 1977, Roberto Peccei and Helen Quinn added a correction term to the theory to cancel  $\mathcal{L}_\theta$  which introduces the Peccei-Quinn symmetry  $U(1)_{PQ}$  to conserve CP in the QCD Lagrangian [9][26].

$$\mathcal{L}_a = \frac{a}{f_a} \frac{g^2}{32\pi^2} F_a^{\mu\nu} \tilde{F}_{a\mu\nu} \quad (2.4)$$

The new  $U(1)_{PQ}$  symmetry is a global symmetry, and under transformations, the transforming parameters (seen in Eq. 2.5) do not require spacetime coordinates and, therefore, do not require fields to be mediated by a gauge field. The  $U(1)_{PQ}$  symmetry is an approximate symmetry that can be spontaneously broken, leading to the emergence of a pseudo-Nambu-

Goldstone boson called the axion. Under a symmetry transformation, the axion field, which is labelled as  $a$ , will transform linearly in the following way:

$$a \rightarrow a + \alpha f_a \quad (2.5)$$

where  $\alpha$  is the global transformation parameter of the  $U(1)_{PQ}$  symmetry, and  $f_a$  is the axion decay constant, which sets the energy scale of PQ symmetry breaking. The axion dynamically relaxes the  $\bar{\theta}$  parameter to zero, potentially resolving the Strong CP Problem. The total QCD Lagrangian would then look like

$$\mathcal{L}_{QCD+a} = \mathcal{L}_{QCD} + \left( \frac{a}{f_a} - \bar{\theta} \right) \frac{g^2}{32\pi^2} F_b^{\mu\nu} \tilde{F}_{b\mu\nu} + \frac{1}{2} \partial^\mu a \partial_\mu a + \mathcal{L}_{int} \quad (2.6)$$

The term  $a/f_a$  functions has a phase (same as  $\bar{\theta}$ ), which can take any value between  $[-\pi, \pi]$ . The value is chosen based on the axion's effective potential and thermal effects. Above a critical temperature of  $T \sim f_a$ , the axion is massless and does not feel an effective potential. As the universe cools below  $f_a$ , the PQ symmetry spontaneously breaks, inducing a non-zero mass for the axion and a corresponding effective potential [27],

$$V(a) = m_a^2 f_{PQ}^2 (1 - \cos [a/f_{PQ}]) \quad (2.7)$$

Initially, the phase  $a/f_a$  can start from any value within  $[-\pi, \pi]$  and will oscillate around the minimum of this potential. These oscillations contribute to the axion behaving as cold dark matter [27]. The axion is a pseudo-Nambu-Goldstone boson, from the spontaneous breaking of the PQ symmetry, which would render it nearly massless if not for the additional interactions with the QCD vacuum because of the topological charge induced by instantons, the axion field gains a small effective mass through interactions with the QCD vacuum's

topological susceptibility ( $\chi_{top}$ ), which quantifies how the energy of the vacuum responds to changes in the topological charge density  $E(\bar{\theta}, T)$  [28] [29].

$$m_a^2(T) f_a^2 = \left. \frac{\partial^2 E(\bar{\theta}, T)}{\partial \bar{\theta}^2} \right|_{\bar{\theta}=0} = \chi_{top}(T) \quad (2.8)$$

Because the mass is generated dynamically, there is no explicit mass term for the axion in the PQ-extended QCD Lagrangian from Eq. 2.6. From lattice QCD, at low temperature, the effective mass term is derived to be [30][31]

$$m_a^2 = \frac{m_u m_d}{(m_u + m_d)^2} \frac{m_\pi^2 f_\pi^2}{f_a^2}, \quad (2.9)$$

where  $m_u$  and  $m_d$  are the up and down quark masses, respectively,  $m_\pi$  is the neutral pion mass, and  $f_\pi = 190$  MeV [10]. The axion's mass is inversely proportional to the axion decay constant  $f_a$ , as seen in Fig. 2.1. Also in Fig. 2.1, astrophysical and cosmological arguments (coloured blue) indicate the ranges of axion masses based on observations such as those related to hot dark matter constraints from the cosmic microwave background (CMB) [32][6] and the Big Bang Nucleosynthesis (BBN)[33], the supernova burst duration from SN1987A, and the behaviour of objects like globular clusters and white dwarfs. Laboratory Searches (coloured gray) and experimental prospects (coloured green) cover regions probed by experiments like ADMX, HAYSTAC, IAXO, CAST, Super-Kamiokande (SK) observations, and solar neutrino flux observations, each targeting different mass ranges. Cavity Experiments, such as the Axion Dark Matter Experiment (ADMX) [34] and the Haloscope at Yale Sensitive to Axion CDM (HAYSTAC) [35], use resonant microwave cavities to detect axions. Additionally, telescope experiments like the CAST experiment [36] use helioscopes, and projects like the International Axion Observatory (IAXO)[37] are part of these advanced searches. Lastly, lattice calculations on the axion field depend on when the PQ symmetry breaking occurs during cosmic inflation. If the PQ symmetry breaks during the pre-inflation era, it happens when the universe is still very small. This early breaking homogenizes the axion field across the observable universe. If PQ symmetry

breaks during the post-inflation era, it occurs when the universe is already large and not uniformly dense, which could result in a non-uniform distribution of the axion field.

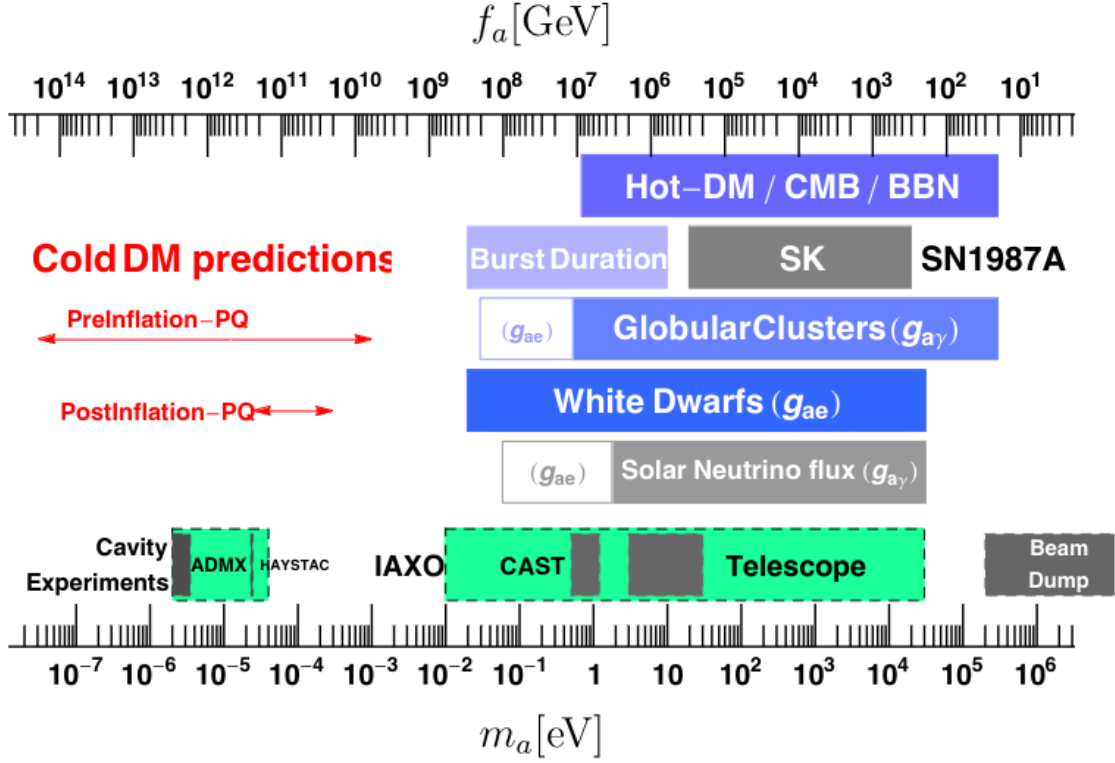


Figure 2.1: Axion mass and decay constant, based on different astronomical observations and experimental efforts, with preinflation and postinflation PQ breaking scenarios calculated using Lattice topology [29].

### 2.0.1 Axion Interactions

The axion is a pseudoscalar that is now a part of the QCD Lagrangian. Therefore, it should be able to couple to other particles like the photon, electron, and other QCD fermions such as quarks and nucleons. Many papers go through the different possible interactions the axion can have with other particles. Eq. 2.10 below showcases the axion-fermion couplings [38][39][40] and Eq. 2.11 showcases the axion-photon coupling [41][42].

$$\mathcal{L}_{aNN} = \frac{C_N}{f_a} \partial_\mu a \bar{\Psi}_N \gamma^\mu \gamma_5 \Psi_N \quad (2.10)$$

$$\mathcal{L}_{a\gamma\gamma} = -\frac{g_{a\gamma\gamma}}{4} a F^{\mu\nu} \bar{F}_{\mu\nu} \quad (2.11)$$

QCD axions can also couple to fermions, including quarks and leptons, through derivative couplings, while the axions couple directly to photons. For this thesis, the most important coupling will be the effective coupling to nucleons, with a coupling constant  $g_{ai}$ , where  $i$  is either a proton or a neutron. The coupling to nucleons is important here because this study is only concerned with axions coming from a nuclear medium at extreme conditions (discussed in section 4). The nucleon-nucleon-axion coupling constant is equal to [43]:

$$g_{ai} = \frac{m_i}{2(f_a/N_{PQ})} \quad (2.12)$$

The coupling contains the nucleon mass ( $m_i$ ) and  $f_a/N_{PQ}$ , where  $N_{PQ}$  is the colour anomaly of the PQ symmetry, which represents the degree to which the PQ symmetry is violated due to QCD effects such as from the gluon self-interactions. The values of  $f_a/N_{PQ}$  have a lower limit of  $f_a/N_{PQ} \geq 8 \times 10^9$  GeV [43]. This coupling appears in nucleon-nucleon-axion bremsstrahlung.

Bremsstrahlung occurs when an initial state of two particles interacts, and then one of the particles radiates energy. The radiation can be a photon, a pair of leptons, or, in the case of this study, the hypothetical axion:

$$\text{Neutrino Bremsstrahlung} \quad N + N \rightarrow N + N + \nu + \bar{\nu} \quad (2.13)$$

$$\text{Axion Bremsstrahlung} \quad N + N \rightarrow N + N + a \quad (2.14)$$

For the nucleon-nucleon-axion bremsstrahlung process, the nucleon interaction can be modelled through one pion exchange. These interactions between nucleons to axions and nucleons to pions come from effective theories [44][45][46],

$$\text{Pion-Nucleon Vertex} \quad (2m_i/m_\pi) f_{ij}\gamma_5, \quad (2.15)$$

$$\text{Axion-Nucleon Vertex} \quad (g_{ai}/m_i) \gamma_5 \phi, \quad (2.16)$$

where Eq. 2.15 and Eq. 2.16 are the vertices when calculating the Feynman diagrams in Fig. 2.2. In the interactions, the indices  $i$  and  $j$  are for the two nucleon flavours, which are either a proton ( $p$ ) or a neutron ( $n$ ), and  $f_{ij}$  are the nucleon pion coupling constant. The constant  $f_{ij}$  depends on the incoming and outgoing nucleons. If the vertex in the Feynman diagram is two neutrons coupling to the pion, then  $f_{nn} \approx 1.05$ , if two protons couple to the pion then  $f_{pp} \approx -1.05$ , and if a neutron and proton couple to the pion then  $f_{np} \approx \sqrt{2}$ , which would correspond to the initial nucleon changing flavours in the final state. These values for  $f_{ij}$  are required to conserve the isospin invariance in the matrix element and are determined from fitting nucleon-nucleon scattering data to the one pion exchange between two nucleons [47]. Additionally,  $g_{ai}$  is the axion-nucleon coupling constant. Even though the axion is considered a Goldstone boson, the interaction includes its slashed momentum  $\not{a} = \gamma^\mu a_\mu$ , exactly like the treatment of fermion momentum in a propagator. This is due to the partial derivative in Eq. 2.10. To go from the Lagrangian density in Eq. 2.10 to Eq. 2.16, the Fourier transform must be taken to go to momentum space. The Feynman rule for the nucleon-nucleon-axion vertex yields,

$$-i \frac{C_N}{f_a} \gamma^\mu a_\mu \gamma_5, \quad (2.17)$$

where  $a_\mu$  is the axion momentum,  $1/f_a \propto g_{ai}/m_i$  (refer to Eq. 2.12), and  $C_N$  is a constant that changes depending on the axion theory used. For this thesis, the QCD axion is investigated, where the axion couples to nucleons.

To study nucleon-nucleon-axion bremsstrahlung, the eight different Feynman diagrams seen in Fig. 2.2 need to be included when calculating the matrix element. The Feynman diagrams are for different permutations of the one-pion exchange between nucleons with

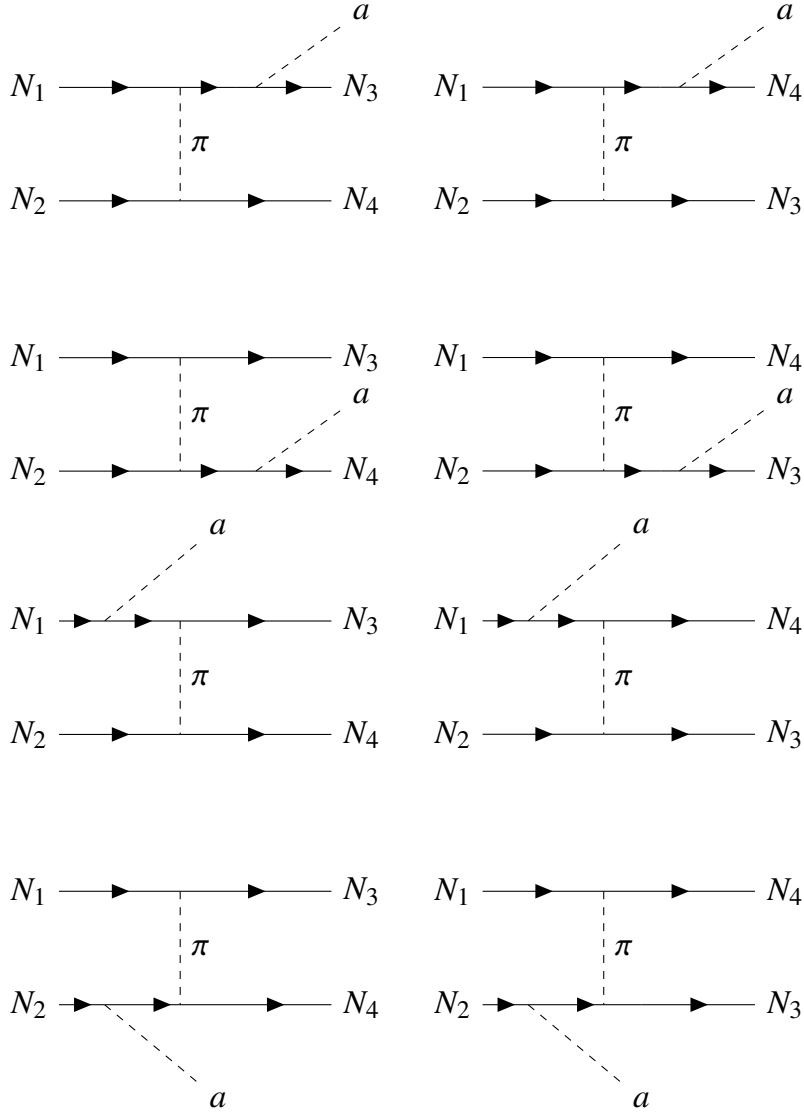


Figure 2.2: Feynman diagrams for nucleon-nucleon-axion bremsstrahlung. There are eight different diagrams to consider, where the couplings to the pion and axion are effective field theory couplings shown in Eq. 2.15 and Eq. 2.16.

an emitting axion, where the long distance interaction between nucleons involves the pion exchanging energy and momentum. After careful calculation, the matrix element is,

$$\sum_{spin} |\mathcal{M}|^2 = \frac{256}{3} \frac{g_{ai}^2 f^4 m_i^2}{m_\pi^4} \left[ \frac{|\vec{k}|^4}{(|\vec{k}|^2 + m_\pi^2)^2} + \frac{|\vec{l}|^4}{(|\vec{l}|^2 + m_\pi^2)^2} + \frac{|\vec{k}|^2 |\vec{l}|^2}{(|\vec{k}|^2 + m_\pi^2)(|\vec{l}|^2 + m_\pi^2)} \right], \quad (2.18)$$

which is in agreement with the calculation performed by Brinkmann and Turner (1988) [44] and Iwamoto [48]. Here  $k = p_1 - p_3$  and  $l = p_2 - p_4$ . In the limit where  $|\vec{k}|^2, |\vec{l}|^2 \gg m_\pi^2$ ,

then the terms in the brackets are approximately equal to 3 and the whole matrix element can be approximated to  $256g_{ai}^2 f^4 m_i^2 / m_\pi^4$ . This condition of  $|\vec{k}|^2, |\vec{l}|^2 \gg m_\pi^2$  occurs when temperatures exceed  $T \geq 6$  MeV [44].

The nucleon-nucleon-axion bremsstrahlung process can occur in a thermal medium of nucleons, such as in a neutron star and neutron star mergers. The next chapter will describe neutron stars and the conditions within them.



## NEUTRON STAR PHYSICS

---

When a massive star with a mass of about  $8 < M/M_{\odot} < 15$  (where  $M_{\odot}$  is the mass of the sun) runs out of fuel so that the pressure generated by the fusion reaction fails to balance the gravitational force, its gravity causes the star to collapse in on itself and a type II supernova occurs, leaving behind an extremely dense stellar object known as a neutron star [49]. Unlike normal stars, which burn nuclear fuel to create thermal pressure, neutron stars mostly use neutron degeneracy pressure to oppose gravity [50]. It is the current understanding that the neutron star has an atmosphere, a solid outer and inner crust, and a neutron-dense outer and inner core (layers of the neutron star can be seen in Fig. 3.1). The outer crust of a neutron star is theorized to be primarily composed of atomic nuclei and electrons, forming a lattice of nuclei immersed in a sea of degenerate electrons [51]. These conditions of high electron degeneracy allow beta capture to occur, where a proton and an electron react to produce a neutron and a neutrino.

Deeper within the neutron star, in the inner crust, the composition includes an increasing number of free neutrons alongside nuclei and electrons. This region comprises nuclei and a neutron fluid, where the isospin asymmetry is high enough for neutrons to begin dripping out of nuclei (the neutrons start to unbind from the nuclei). The drip density, which is approximately the start of the inner crust, is about  $n_{drip} \approx 2 \times 10^{-3} n_0$ , where  $n_0 \approx 0.15 \text{ fm}^{-3}$  is the nuclear saturation density [51]. When the medium consists of infinite nuclear matter, saturation density occurs at the point where protons and neutrons reach their minimum energy per nucleon [52]. At these high densities, the phenomenon of "nuclear pasta" occurs, primarily in the inner crust. This unique structure arises from the balance between the strong nuclear force binding protons and neutrons and the Coulomb repulsion between protons. As

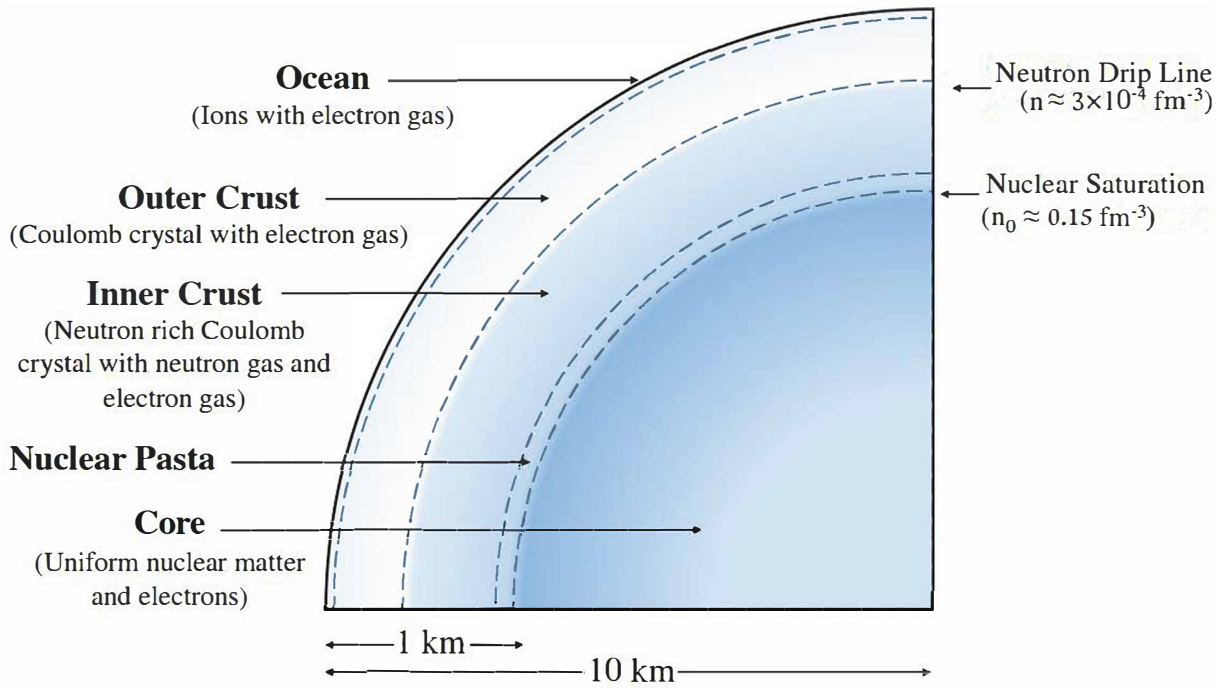


Figure 3.1: The layers of a typical neutron star [53].

a result, nuclei start to deform, no longer resembling their spherical shapes but stretching and connecting with neighbours. This deformation leads to various pasta-like phases such as blob-like "gnocchi" shapes, elongated rod-like "spaghetti," flattened "lasagna" sheets, and void-filled "Swiss cheese" structures [53].

Further inward, the outer core of the neutron star is primarily composed of free neutrons, with a smaller proportion of protons and electrons. The density in this region reaches past saturation density,  $n \geq n_0$  [53]. The inner core's composition remains uncertain, with theories suggesting exotic forms of matter. Hyperons (which are baryons that contain a strange quark) [54], or the neutrons reaching a superfluid state (when neutrons form Cooper pairs) [55], or quark-matter [56], may occur within the core.

### 3.0.1 Neutron Star Cooling

Lowering the temperature of a neutron star requires energy to be carried out, and only particles with a long enough mean free path (labelled  $\lambda$ ) are able to escape. To be emitted by

the neutron star, a neutrino's mean free path is likely larger than the radius of a neutron star, which can range from  $R \sim (10 - 15)$  km. When neutrinos are the thermal energy carriers that cool the neutron star, this is commonly known as the Urca process (named after a casino in Rio de Janeiro, called Casino da Urca, because the "... Urca Process results in a rapid disappearance of thermal energy from the interior of a star, similar to the rapid disappearance of money from the pockets of the gamblers on the Casino da Urca", as stated by George Gamow in 1970 [57]). The Urca process involves the emission of neutrinos and antineutrinos through decays within the star [57].

$$\text{Beta Decay} \quad n \rightarrow p + e^- + \bar{\nu}_e \quad (3.1)$$

$$\text{Beta Capture} \quad p + e^- \rightarrow n + \nu_e \quad (3.2)$$

Eqs. (3.1)-(3.2) are known as direct Urca (dUrca) processes since there is only one nucleon involved at the initial and final states.

For beta decay to occur, there must be enough available final unoccupied Fermi states for the electrons and protons. Therefore, the energy and momentum on the Fermi surface of the particles must satisfy  $p_{pF} + p_{eF} \geq p_{nF}$  for the reaction to occur [58]. The Fermi momentum is related to the number density ( $n_i$ ) in the low-temperature limit:

$$n_i = \int g \frac{d^3 p_i}{(2\pi)^3} \Theta(p_{iF} - p_i) \quad (3.3)$$

Here,  $i$  is the species of the fermion (either  $i = n, p$ , or  $e$ ),  $g = 2s + 1$  is the degeneracy factor and  $s = 1/2$  is the spin of the particle, resulting in  $g = 2$ , and  $\Theta(p_{iF} - p_i)$  is the step-function which represents the distribution of particles at  $T \rightarrow 0$ :

$$\rightarrow = \int_0^{p_{iF}} (2) \frac{4\pi p_i^2 dp_i}{(2\pi)^3} \quad (3.4)$$

$$= \frac{p_{iF}^3}{3\pi^2} \quad (3.5)$$

Therefore, the relation between density and Fermi momentum is  $p_{iF} = (3\pi^2 n_i)^{1/3}$ . The abundance of electrons is high in the neutron star, making there enough final electron states for beta decay to occur. The neutron star is charge-neutral, so the number density of electrons must equal the number density of protons. Therefore, the inequality  $p_{pF} + p_{eF} \geq p_{nF}$  then becomes,

$$p_{pF} + p_{eF} \geq p_{nF} \quad (3.6)$$

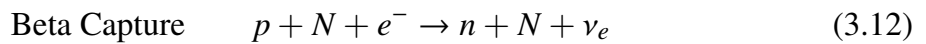
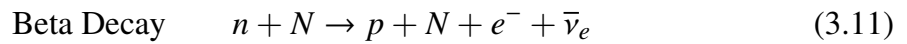
$$(3\pi^2 n_p)^{1/3} + (3\pi^2 n_e)^{1/3} \geq (3\pi^2 n_n)^{1/3} \quad n_p = n_e \quad (3.7)$$

$$8n_p \geq n_n \quad \text{let } n = n_p + n_e \quad (3.8)$$

$$9n_p/n \geq 1 \quad (3.9)$$

$$\therefore n_p/n \geq 1/9 \quad (3.10)$$

where  $n_n$  is the number density for neutrons,  $n_p$  is the number density for protons,  $n_e$  is the number density for electrons, and  $n$  is the nucleon density. Therefore, there must be enough protons (more than  $1/9 = 11\%$  of the total density) in the neutron star for dUrca, or else the Pauli exclusion principle will stop the reaction from moving forward. However, at high temperatures, degenerate fermions have lots of energy and, therefore, have lots of states available, so the Pauli exclusion principle is of little concern. In the modified Urca (mUrca) process, the presence of an additional nucleon alleviates the constraints imposed by density since the spectator nucleon facilitates the conservation of momentum without needing the high proton densities [57].



For mUrca, the additional nucleon can act as a momentum source or sink in order to conserve the momentum. When  $N = n$ , there is no threshold density, and when  $N = p$ , the spectator

proton adds two additional Fermi momenta in the equality,  $3p_{pF} + p_{eF} > p_{nF}$ , which requires much less protons in the neutron star compared to dUrca ( $n_p/n \geq 1/65$  or 1.5% of the total density must be protons) [59][57].

### 3.0.2 Conditions during Neutron Star Mergers

At high temperatures of about  $T \approx 5$  MeV, even neutrinos become trapped in the medium. Therefore, investigating the axion, which couples more weakly to nucleons, may become an important process in the neutron star's luminosity [60]. Neutrinos may become trapped in the neutron star because the mean free path of neutrinos may be smaller than the radius at these high temperatures. In general, the mean free path can be expressed as [50]

$$\lambda = \frac{1}{n\sigma}, \quad (3.14)$$

where  $\sigma$  is the neutrino-nucleon cross-section. The effective mean free path is calculated based on inelastic and elastic scattering reactions at saturation density [50]

$$\lambda_{eff} \sim 2.5 \times 10^5 \text{ km} \left( \frac{0.1 \text{ MeV}}{E_\nu} \right)^{5/2}. \quad (3.15)$$

If the neutrino's energy is approximately  $E_\nu \sim kT$ , (in natural units  $k = 1$ ), then at around  $T = 10$  MeV,  $\lambda_{eff} \approx 2.5$  km. Since the typical radius of a neutron star is around  $R \sim (10 - 15)$  km, the neutrinos can be trapped at these higher temperatures. Certain reactions can cause the neutrino to be absorbed in the medium, and these reactions are used to calculate the mean free path of the neutrino. However, these absorptions may only occur if the conditions, such as temperature and density, satisfy the reaction. The higher the temperature, the more frequently these reactions can occur [61]. In neutron star mergers, the temperature can reach extreme conditions, around  $T = 5 - 50$  MeV[62] [63]. Therefore, studying the axions and neutrinos may help reveal the neutron star merger dynamics.

In section 5, the calculations of nucleon-nucleon-axion bremsstrahlung emissivities at  $T = 6$  MeV, 10 MeV, and 50 MeV will be strategically chosen to probe the efficiency of axion emissions. At 10 MeV, the environment is optimal for significant neutrino trapping, which suggests a high-density scenario where axion bremsstrahlung could also be notably effective. Temperatures of 6 MeV provide insight into less extreme conditions and are the threshold where our approximations for the matrix element ( $|\mathcal{M}|^2$ ) from Eq. 2.18 hold. Lastly, 50 MeV is chosen because the extreme conditions of some neutron star mergers can reach this temperature, and the axion emissivity might drastically change at this increased energy and density.

### 3.0.3 Neutron Star Equation of State

A simple model for the nuclear matter inside of a nucleus or neutron star is made of an SU(2) isospin doublet

$$\psi = \begin{pmatrix} p \\ n \end{pmatrix} \quad (3.16)$$

where the particles in the doublet are either isospin  $I_z = \frac{1}{2}$  for the proton, or  $I_z = -\frac{1}{2}$  for the neutron. It will be shown that the number density  $n_i$  of each nucleon will affect the energies in the system, especially if the number densities of the two nucleons are unequal. Considering  $A = N + Z$  nucleons, where  $N$  is the number of neutrons and  $Z$  is the number of protons, all interacting together from the strong nuclear force which affected the energy of the system, ie. the mass of the nucleus or the energy of the nucleons in infinite nuclear matter [64],

$$E(Z, A) = -a_v A + a_s A^{2/3} + a_c Z^2 A^{-1/3} - a_A \frac{(N - Z)^2}{A} + \frac{(-1)^Z + (-1)^N}{2} a_p A^{-1/2}. \quad (3.17)$$

In this expression,  $a_V$  is the volume term that accounts for the interactions between interior nucleons,  $a_S$  is the surface term that accounts for the nucleons on the surface of the medium that don't have the same amount of nearest neighbours as interior nucleons,  $a_C$  is the Coulomb term for the protons interacting with each other,  $a_P$  is the pairing term which accounts for nucleons being alone in an energy level or with a pair in an energy level, and  $a_A$  is the asymmetry term which accounts for the isospin asymmetry. For infinite nuclear matter, we can study the energy of the system by letting  $N$ ,  $Z$ , and  $A$  go to infinity, ignoring the surface term and Coulomb term since there is no boundary in this approximation and because of the charge neutrality of our medium. Let us define  $\delta$  as the term that quantifies the energy cost related to the difference in neutron number densities ( $n_n$ ) to proton number densities ( $n_p$ ):

$$\delta = \frac{N - Z}{A} = \frac{n_n - n_p}{n}, \quad \text{where} \quad n = \frac{A}{V} = \frac{N + Z}{V} = n_n + n_p. \quad (3.18)$$

When  $\delta = 0$  we have symmetric nuclear matter, and when  $\delta = 1$  the medium is purely made of neutrons. By expressing the energy in terms of  $E(n, \delta)/A$  and Taylor expanding the expression around  $\delta = 0$  [65],

$$E(n, \delta)/A = E(n, 0)/A + \left( \frac{\partial E(n, \delta)/A}{\partial \delta} \right)_{\delta=0} \delta + \frac{1}{2} \left( \frac{\partial^2 E(n, \delta)/A}{\partial \delta^2} \right)_{\delta=0} \delta^2 + \dots \quad (3.19)$$

The first partial derivative of  $E(n, \delta)/A$  is zero when  $\delta = 0$  due to the isospin symmetry of the nuclear force. Therefore, the strong interaction energy between two neutrons is essentially the same as that between two protons. The second derivative in this expansion is defined as

$$S(n) = \frac{1}{2} \left( \frac{\partial^2 E(n, \delta)/A}{\partial \delta^2} \right)_{\delta=0} \quad (3.20)$$

which is called the symmetry energy: the difference in energy per nucleon between pure neutron matter and symmetric nuclear matter. It quantifies the energy cost associated with deviating from the condition of equal numbers of protons and neutrons.

$$S(n) \approx E(n, \delta = 1)/A - E(\delta = 0)/A \approx E_{PNM} - E_{SNM} \quad (3.21)$$

Mathematically, the symmetry energy  $S(n)$  as a function of nuclear matter density  $n = n_n + n_p$  can be expressed and expanded around the saturation density  $n_0$  as follows [66],

$$S(n) = J + L \left( \frac{n - n_0}{3n_0} \right) + \frac{1}{2} K_{sym} \left( \frac{n - n_0}{3n_0} \right)^2 + \dots \quad (3.22)$$

Here,  $J$  represents the symmetry energy at the saturation density  $n_0$ , and  $L$  is the slope parameter that indicates how the symmetry energy changes with the density of the nuclear matter. Saturation density is when nuclear matter reaches a balance between attractive and repulsive forces, resulting in a stable, minimal energy configuration. At this density, the symmetry energy  $J$  is the additional energy per nucleon required to convert symmetric nuclear matter into pure neutron matter. The parameter  $L$  is known as the density slope of the symmetry energy and is defined as

$$L = 3n_0 \left. \frac{\partial S(n)}{\partial n} \right|_{n=n_0}. \quad (3.23)$$

This parameter quantifies the first-order change in the symmetry energy with respect to changes in the nuclear matter density around the saturation point. The slope is directly proportional to the pressure of pure neutron matter (PNM), which corresponds to  $\delta = 1$ . This relation is [67]

$$P_0 \approx \frac{1}{3} n_0 L. \quad (3.24)$$

A higher value of  $L$  indicates a more rapid increase in symmetry energy with density, leading to a stiffer equation of state. This has profound implications for the properties of neutron stars, including their maximum mass and radius [68]. Another important constant is  $K_{sym}$ , which represents the curvature of the symmetry energy at saturation density. It is defined as

$$K_{sym} = 9n_0^2 \left. \frac{\partial^2 S(n)}{\partial n^2} \right|_{n=n_0}. \quad (3.25)$$

The curvature  $K_{sym}$  provides insight into the second-order change in the symmetry energy with respect to the nuclear matter density around the saturation point.

The equation of state used in this thesis is a popular nucleonic equation of state: FSUGold2. It has been calibrated to the properties of infinite nuclear matter and the ground state properties of finite nuclei [69]. The equation of state lists the Landau effective masses  $m^*$  (defined in Eq. 3.30) of neutrons and protons at different particle densities in a tabular form. The Lagrangian density for this equation of state is  $\mathcal{L} = \mathcal{L}_0 + \mathcal{L}_{int}$ , where

$$\begin{aligned} \mathcal{L}_0 = & \bar{\psi} (i\gamma^\mu \partial_\mu - M) \psi + \frac{1}{2} (\partial_\mu \phi \partial^\mu \phi - m_s^2 \phi^2) + \frac{1}{2} m_v^2 V_\mu V^\mu - \frac{1}{4} F_{\mu\nu} F^{\mu\nu} \\ & + \frac{1}{2} m_\rho^2 \mathbf{b}_\mu \cdot \mathbf{b}^\mu - \frac{1}{4} V_{\mu\nu} V^{\mu\nu} - \frac{1}{4} \mathbf{b}_{\mu\nu} \cdot \mathbf{b}^{\mu\nu}. \end{aligned} \quad (3.26)$$

The interaction terms for the Lagrangian are,

$$\begin{aligned} \mathcal{L}_{int} = & \bar{\psi} \left[ g_s \phi - \left( g_v V_\mu + \frac{g_\rho}{2} \boldsymbol{\tau} \cdot \mathbf{b}_\mu + \frac{e}{2} (1 + \tau_3) A_\mu \right) \gamma^\mu \right] \psi \\ & - \frac{\kappa}{3!} (g_s \phi)^3 - \frac{\lambda}{4!} (g_s \phi)^4 + \frac{\zeta}{4!} (g_v^2 V_\mu V^\mu)^2 + \Lambda_v (g_\rho^2 \mathbf{b}_\mu \cdot \mathbf{b}^\mu) (g_v^2 V_\mu V^\mu). \end{aligned} \quad (3.27)$$

In Eq. 3.26 and Eq. 3.27,  $\psi$  is the isospin double field for the nucleons from Eq. 3.16,  $\phi$  is the isoscalar-scalar  $\sigma$ -meson field,  $V_\mu$  is the scalar-vector  $\omega$ -meson field,  $\mathbf{b}_\mu$  is the isovector-vector  $\rho$ -meson field, and  $A_\mu$  is the photon field.  $\boldsymbol{\tau}$  are the Pauli matrices and  $\boldsymbol{\gamma}^\mu$  are the gamma matrices. The mass terms  $m_s$ ,  $m_v$  and  $m_\rho$  are for the  $\sigma$ -meson mass, the  $\omega$ -meson mass and  $\rho$ -meson mass, respectively. The Yukawa coupling constants are  $g_s$ ,  $g_v$ ,  $g_\rho$  and  $e$  which are to couple the  $\sigma$ -meson, the  $\omega$ -meson, the  $\rho$ -meson, and the photon to nucleons,

respectively. The coefficients  $\kappa$ ,  $\lambda$ ,  $\zeta$ , and  $\Lambda_v$  are associated with the meson interactions, which affect the equation of state. To reduce  $K_{sym}$ , the  $\kappa$ ,  $\lambda$  coefficients were introduced into the Lagrangian,  $\zeta$  is used to tune neutron star observables such as the mass, and  $\Lambda_v$  is sensitive to the slope  $L$  [69].

Fig. 3.2 is taken from ref. [65] and shows the energy per nucleon from Eq. 3.19 in terms of the Fermi momentum of the nucleons, where  $k_F = (\frac{3}{2}\pi^2 n)^{1/3}$  (the factor of 1/2 comes from the fact that both proton and neutron densities are considered). What is analyzed is how the difference between neutron and proton fractions,

$$Y_i = n_i / (n_n + n_p) \quad \text{and} \quad 1 = Y_n + Y_p, \quad (3.28)$$

changes the energy per nucleon and showcases the minimum energy at saturation density using the FSUGold2 equation of state [65]. The proton fraction is related to  $\delta$  by,

$$\delta = Y_n - Y_p = 1 - 2Y_p. \quad (3.29)$$

The Landau effective mass is modified by interactions with other particles in the Lagrangian. The Landau effective mass, which is denoted as  $m_i^*$  ( $i$  =neutron or proton), is defined as

$$m_i^* = \sqrt{k_{iF}^2 + m_{Dirac,i}^2}, \quad (3.30)$$

where  $k_{iF} = (3\pi n_i)^{1/3}$  (refer back to Eq. 3.5), and  $m_{Dirac,i}$  is the effective mass taken from the Dirac equation, which is derived from finding the equation of motion for the nucleon field from the Lagrangian:

$$\frac{\partial}{\partial x^\mu} \left( \frac{\partial \mathcal{L}}{\partial (\partial^\mu \psi)} \right) - \frac{\partial \mathcal{L}}{\partial \psi} = 0 \quad (3.31)$$

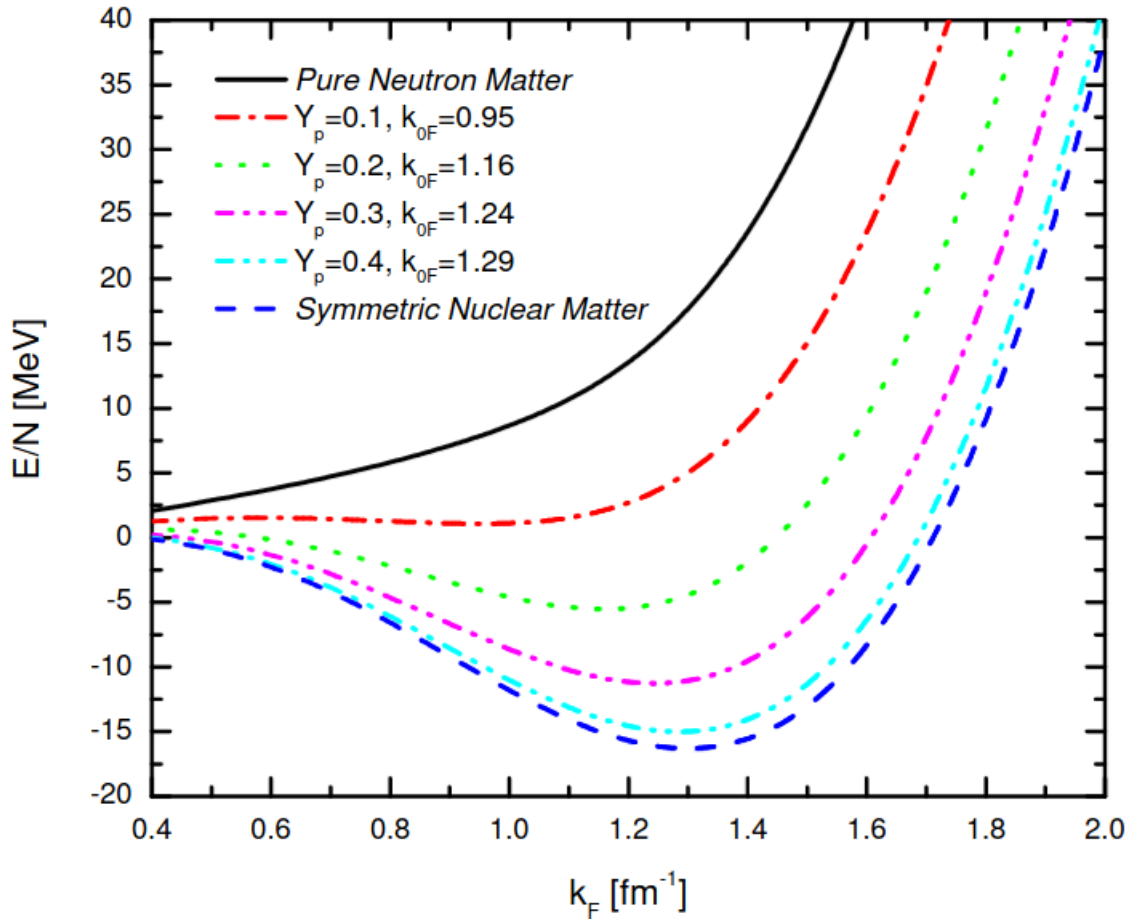


Figure 3.2: The energy per nucleon calculated using the FSUGold2 equation of state at different densities and different proton fractions, where  $k_F = (\frac{3}{2}\pi^2 n)^{1/3}$  and is the nucleon density  $n = n_n + n_p$  [65].

The result from the Euler-Lagrange equation is,

$$\left[ \gamma^\mu \left( i\partial_\mu - g_v V_\mu - \frac{g_\rho}{2} \boldsymbol{\tau} \cdot \mathbf{b}_\mu \right) - (M - g_s \phi) \right] \psi = 0. \quad (3.32)$$

This is the Dirac equation, with the effective mass equalling  $m_{Dirac} = M - g_s \phi$ . The interaction with the  $\sigma$ -meson reduces the Dirac mass from the bare mass, and then the Landau effective mass increases as the density is increased, with the proportionality  $m_i^* \propto n_i^{1/3}$ . For the rest of this thesis, the Landau effective mass will just be referred to as the effective mass.

## Part II

### CALCULATING THE AXION EMISSIVITY



## EMISSIVITY THROUGH BREMSSTRAHLUNG

---

For a system of many particles, there can be many different interactions occurring at the same time. Therefore, all possible interactions must be considered, and all their possible outgoing momentum and energy must be integrated. This section will go over the process of calculating particle interactions by calculating the phase space integrals for relativistic binary collisions. The phase space integrals will then be used to calculate the rate of reactions and emissivities for bremsstrahlung processes.

### 4.0.1 *Kinematics*

We will use the Minkowski metric commonly used for high-energy particle physics. This metric is the mostly negative metric convention, where the scalar term is positive, and the vector terms are negative:

$$g^{\mu\nu} = \text{diag}(1, -1, -1, -1). \quad (4.1)$$

With this convention, the four-momentum  $p^\mu = (E, \mathbf{p})$  has a squared magnitude equal to the positive invariant mass squared for the particle,

$$p^\mu p_\mu = E^2 - |\mathbf{p}|^2 = M^2. \quad (4.2)$$

The Lorentz invariant phase space differential element for  $n$  particles used to integrate over all possible degrees of freedom is

$$d\Phi^n(p_1, \dots, p_n) = \prod_{i=1}^n \frac{d^3 p_i}{(2\pi)^3 2E_i} \delta^3\left(\sum_{i=1}^n \mathbf{p}_i\right) \delta\left(\sum_{i=1}^n E_i\right) \quad (4.3)$$

The rate of interactions between an initial state and a final state of particles will then be given by the integral of the matrix element squared. The matrix element squared  $|\overline{\mathcal{M}}|^2$  and the phase space element together then make up the rate equation,

$$\mathcal{R} = \int |\overline{\mathcal{M}}|^2 d\Phi^n \quad (4.4)$$

$$= \int |\overline{\mathcal{M}}|^2 (2\pi)^4 \delta^3\left(\sum_{i=1}^n \mathbf{p}_i\right) \delta\left(\sum_{i=1}^n E_i\right) \prod_{i=1}^n \frac{d^3 p_i}{(2\pi)^3 2E_i} \quad (4.5)$$

The delta functions are in place to conserve energy and momentum in the collision, which can be used to integrate out some dimensions in the phase space integral. For processes that involve  $2 \rightarrow 2$  collisions, an analytic solution can be determined because of the simplicity of the spin-average matrix element, while any collision process that involves more particles in the system, a numerical calculation will be needed [70].

When integrating the square of the matrix element, the rate shows the probability ( $P$ ) of an event per volume ( $V$ ) per time ( $t$ ), and in natural units has a dimension of  $E^4$ , where  $E$  is energy,

$$\mathcal{R} = \frac{dP}{dV dt} = \frac{dP}{d^4 x} \quad (4.6)$$

The simple two-body scattering case can be derived using the thermal averaged cross-section to calculate the reaction rate in gases and thermal mediums. To derive the rate of reaction, the effective area of the target particle is first needed:

$$n_i \sigma V \quad (4.7)$$

where  $n_i$  is the number density of the target,  $\sigma$  is the cross-section, and  $V$  is the volume. By multiplying by the flux of incoming particles  $n_j v$ , then the reaction rate will be equal to:

$$n_i v n_j \sigma V \quad (4.8)$$

To get the rate reaction seen from Eq. 4.6, we divide by volume, making the rate of reaction,  $r$ , to equal:

$$r = n_i v n_j \sigma \quad (4.9)$$

Thus, the thermal averaged cross-section can be calculated using the velocity distribution,

$$\int_0^{\infty} dv \phi(v) = 1. \quad (4.10)$$

Therefore, the thermal averaged cross-section, which is related to the reaction rate, is equal to,

$$\langle \sigma v \rangle = \int_0^{\infty} dv \phi(v) \sigma v, \quad (4.11)$$

and the reaction rate similar to Eq. 4.6 is equal to

$$\mathcal{R} = \frac{1}{1 + \delta_{ij}} n_i n_j \langle \sigma v \rangle, \quad (4.12)$$

where the  $\delta_{ij}$  is either 0 or 1 based on whether the target particle and incoming particle are identical or not, to account for double counting. Eq. 4.12 is the classical reaction rate for particle collisions. To account for quantum interactions, the distribution of particles in the thermal medium will be the phase space distribution functions. Either the Fermi-Dirac

distribution or the Bose-Einstein distribution will be used for fermions or bosons in the thermal medium, respectively.

$$f = \frac{1}{\exp[(E - \mu) / T] \pm 1} \quad \text{Fermions (+)} \quad \text{Bosons (-)} \quad (4.13)$$

The distribution function represents the probability that the initial particle occupies a quantum state [71]. The thermal distribution depends on the energy, temperature, and chemical potential  $\mu$  of the medium. At absolute zero, the chemical potential of a Fermi gas is equal to the Fermi energy,  $\mu = E_F$ . In the integral from Eq. 4.5, the terms for the incident particles are just  $f(E_i, \mu_i)$ , while the outgoing particles are  $[1 \mp f(E_i, \mu_i)]$ , for fermions (-) and bosons (+), respectively. The  $(1 - f)$  factor for final fermions represents the number of empty states in the final phase space since they must obey the Pauli exclusion principle, while the  $(1 + f)$  factor for final bosons represents the Bose-Einstein enhancement for the final states, which is the attraction between bosons to fill the same quantum state [71]. Therefore, the reaction rate for a system of particles is

$$\mathcal{R} = \int |\overline{\mathcal{M}}_n|^2 (2\pi)^4 \delta^3 \left( \sum_{i=1}^n \mathbf{p}_i \right) \delta \left( \sum_{i=1}^n E_i \right) \prod_{i=1}^n \frac{d^3 p_i}{(2\pi)^3 2E_i} \prod_{i=1}^n f_i \prod_{i=j}^m (1 \mp f_j) \quad (4.14)$$

However, to calculate emissivities, this process involves finding the amount of energy that is carried out of the system. Therefore, the energy of the particle of interest will also be included in the integral, and the emissivities show the number of energy-carrying events per volume per time;

$$\dot{\epsilon} = \frac{dE}{dV dt} = \frac{dE}{d^4 x} \quad (4.15)$$

with dimensions equal to  $E^5$ .

#### 4.0.2 Neutrino Bremsstrahlung Rates

In this thesis, the neutrino rates for nucleon-nucleon-neutrino bremsstrahlung will be compared to nucleon-nucleon-axion bremsstrahlung. The Lorentz invariant emissivity of neutrinos from a  $N_1 + N_2 \rightarrow N_3 + N_4 + \nu + \bar{\nu}$  reaction in a medium of nucleons is then

$$\begin{aligned} \dot{\epsilon}^{(NN)} = & \int \left[ \prod_{j=1}^4 \frac{d^3 p_j}{(2\pi)^3} \right] \frac{d^3 p_\nu}{(2\pi)^3} \frac{d^3 p'_\nu}{(2\pi)^3} \omega_\nu (2\pi)^4 \delta(E_f - E_i) \delta^3(\mathbf{p}_f - \mathbf{p}_i) \\ & \times f_1 f_2 (1 - f_3) (1 - f_4) \mathcal{S} |\mathcal{M}_{fi}|^2 \end{aligned} \quad (4.16)$$

where  $f_1$  and  $f_2$  correspond to the incoming nucleons  $N_1$  and  $N_2$ , and  $1 - f_3$  and  $(1 - f_4)$  correspond to the final nucleons  $N_3$  and  $N_4$ . The difference between Eq. 4.16 and Eq. 4.14 is the included neutrino energy  $\omega_\nu = E_\nu + E_{\bar{\nu}}$ . The final expressions for the neutrino emissivities is [57]:

$$\begin{aligned} \dot{\epsilon}^{(nn)} = & \frac{41}{14175} \frac{G_F^2 g_A^2 m_n^{*4}}{2\pi\hbar^{10} c^8} \left( \frac{f_{nn}}{m_\pi} \right)^4 p_{nF} \alpha_{nn} \beta_{nn} (kT)^8 \mathcal{N}_\nu \\ \approx & 2.35 \times 10^{-28} \left( \frac{m_n^*}{m_n} \right)^4 \left( \frac{n_n}{n_0} \right)^{1/3} T_9^8 \text{ MeV}^5 \end{aligned} \quad (4.17)$$

$$\begin{aligned} \dot{\epsilon}^{(pp)} = & \frac{41}{14175} \frac{G_F^2 g_A^2 m_p^{*4}}{2\pi\hbar^{10} c^8} \left( \frac{f_{pp}}{m_\pi} \right)^4 p_{pF} \alpha_{pp} \beta_{pp} (kT)^8 \mathcal{N}_\nu \\ \approx & 5.47 \times 10^{-29} \left( \frac{m_p^*}{m_p} \right)^4 \left( \frac{n_p}{n_0} \right)^{1/3} T_9^8 \text{ MeV}^5 \end{aligned} \quad (4.18)$$

The nucleon-nucleon-neutrino bremsstrahlung rates are in units of  $E^5$  and depend on the effective mass  $m_i^*$  and number density  $n_i$  of the nucleons. Eq. 4.17 is for  $n + n \rightarrow n + n + \nu + \bar{\nu}$ , while Eq. 4.18 is for  $p + p \rightarrow p + p + \nu + \bar{\nu}$ . In these expressions,  $G_F = 1.17 \times 10^{-11} \text{ MeV}^{-2}$  is the Fermi constant which comes from the weak interactions to neutrinos,  $g_A = 1.26$  is the nucleon axial-vector constant [72],  $f_{nn}$  and  $f_{pp}$  are defined the same as from the discussion below Eq. 2.15,  $m_\pi = 135 \text{ MeV}$  is the pion mass,  $m_n = 940 \text{ MeV}$  is the neutron bare mass, and  $m_p = 938 \text{ MeV}$  is the proton bare mass. The terms  $\alpha_{ii}$  and  $\beta_{ii}$  are correction factors to account for effects not included in the square matrix element,

such as repulsive nucleon-nucleon corrections, etc [57]. Note that  $\mathcal{N}_\nu = 3$  is the number of neutrino flavours that we are considering, and the term  $T_9 = T / (10^9\text{K})$  is the temperature. Lastly,  $p_{iF}$  is the nucleon's Fermi momentum, which is related to the number density by the proportionality is  $p_{iF} \propto n_i^{1/3}$  (refer back to Eq. 3.5), which can be seen in Eqs. 4.17 and 4.18.

### 4.0.3 Axion Bremsstrahlung Rates

This section shows the derivation for nucleon-nucleon-axion bremsstrahlung emissivity. The emission rate of axions in an environment full of nucleons needs to take into account the effective masses, as well as the many-body and multiple-scattering effect. The axion is a boson, so one uses the Bose-Einstein distribution from Eq. 4.13. However, since we will assume the axion is freely escaping the medium without interacting, the term  $(1 + f_a)$  can be ignored since the axion is "free-streaming". The nucleon-nucleon-axion bremsstrahlung emission rates are

$$\dot{\epsilon} = \int d\Pi_1 d\Pi_2 d\Pi_3 d\Pi_4 d\Pi_a (2\pi)^4 \mathcal{S} |\mathcal{M}|^2 \delta^4(p_1 + p_2 - p_3 - p_4 - p_a) E_a f_1 f_2 (1 - f_3)(1 - f_4), \quad (4.19)$$

where the differential element for each particle is

$$d\Pi_i = \frac{d^3 p_i}{(2\pi)^3 2E_i}. \quad (4.20)$$

The Fermi-Dirac distribution for the particles in a thermal medium is

$$f_i = \frac{1}{e^{E_i/T - \mu_i/T} + 1}, \quad (4.21)$$

where the energy is integrated and the chemical potential is inserted into the integral from the density of the particles, shown in Eq. 4.43 and Eq. 4.50.

The constant  $\mathcal{S}$  is the symmetry term, which can be included when calculating the matrix element  $|\overline{\mathcal{M}}|^2$ , but is left kept outside for this expression. To account for identical particles in the final state, the symmetry factor is  $\mathcal{S} = \frac{1}{N!} = \frac{1}{2!}$  for two identical nucleons (for this calculation, we will not be considering the  $n + p \rightarrow n + p + a$  reaction, and leave it up for future works). Using the following change of variables,

$$\vec{p}_{\pm} = \frac{\vec{p}_1 \pm \vec{p}_2}{2}, \quad \vec{p}_{3c/4c} = \vec{p}_{3/4} - \vec{p}_+ \quad (4.22)$$

at these densities, the non-relativistic limit for all the particles is a good approximation, and we can assume some of the energies to be approximately

$$E_i = m_i^* + \frac{p_i^2}{2m_i^*} \approx m_i^*. \quad (4.23)$$

Additionally, the momentum of the axion compared to the heavier nucleons can be approximated to equal  $\vec{p}_a \approx 0$ , making the other terms in the expression equal

$$\vec{p}_{3c} = -\vec{p}_{4c} \quad (4.24)$$

$$E_a = |p_a| \quad (4.25)$$

$$\therefore d^3 p_a = 4\pi E_a^2 dE_a \quad (4.26)$$

To simplify the expression, the following part can be simplified through the following steps,

$$\mathcal{S} \int \frac{d^3 p_1}{(2\pi)^3 2E_1} \frac{d^3 p_2}{(2\pi)^3 2E_2} \frac{d^3 p_3}{(2\pi)^3 2E_3} \frac{d^3 p_4}{(2\pi)^3 2E_4} \frac{d^3 p_a}{(2\pi)^3 2E_a} E_a \quad (4.27)$$

$$\times (2\pi)^4 \delta^4(p_1 + p_2 - p_3 - p_4 - p_a)$$

$$= \frac{1}{32(2\pi)^{11}} \int \frac{d^3 p_1}{m_i^*} \frac{d^3 p_2}{m_i^*} \frac{d^3 p_3}{m_i^*} \frac{d^3 p_4}{m_i^*} d^3 p_a \delta^3(\vec{p}_1 + \vec{p}_2 - \vec{p}_3 - \vec{p}_4) \quad (4.28)$$

$$\times \delta(E_1 + E_2 - E_3 - E_4 - E_a)$$

The  $d^3 p_4$  term can be evaluated with the momentum delta function, which would make the momentum and energy of  $p_4$  equal

$$\vec{p}_4 = \vec{p}_1 + \vec{p}_2 - \vec{p}_3, \quad \text{and} \quad E_4 = m_i^* + \frac{(\vec{p}_1 + \vec{p}_2 - \vec{p}_3)^2}{2m_i^*}. \quad (4.29)$$

Therefore, the expression then is currently

$$= \frac{1}{32(2\pi)^{11}} \frac{1}{(m_i^*)^4} \int d^3 p_1 d^3 p_2 d^3 p_3 d^3 p_a \delta(E_1 + E_2 - E_3 - E_4 - E_a). \quad (4.30)$$

With  $d^3 p_a = 4\pi E_a^2 dE_a$ , we can evaluate  $dE_a$  with the energy delta function as well,

$$= \frac{4\pi}{32(2\pi)^{11} (m_i^*)^4} \int d^3 p_1 d^3 p_2 d^3 p_3 E_a^2, \quad (4.31)$$

and when  $\vec{p}_a = 0$ ,

$$E_a = \frac{p_-^2 - p_{3c}^2}{m_i^*} \quad (4.32)$$

The following steps are to change the differential elements in the integral to our new variables from Eq. 4.22,

$$\mathcal{J} d^3 p_1 d^3 p_2 d^3 p_3 = d^3 p_+ d^3 p_- d^3 p_{3c} = (2\pi p_+^2 dp_+ d\gamma) (4\pi p_-^2 dp_-) (2\pi p_{3c}^2 dp_{3c} d\gamma_c) \quad (4.33)$$

$$\text{with} \quad \mathcal{J} = \frac{1}{8} \quad (4.34)$$

Here,  $\gamma$  and  $\gamma_c$  are defined as

$$\gamma = \frac{\vec{p}_+ \cdot \vec{p}_-}{|\vec{p}_+| |\vec{p}_-|} \quad \gamma_c = \frac{\vec{p}_+ \cdot \vec{p}_{3c}}{|\vec{p}_+| |\vec{p}_{3c}|} \quad (4.35)$$

Changing the momentum terms to dimensionless energy terms,

$$u_i = \frac{p_i^2}{2m_i^*T} \quad \mathcal{J} dp_+ dp_- dp_{3c} = du_+ du_- du_{3c}, \quad (4.36)$$

the Jacobian matrix simplifies the integral to

$$\mathcal{J} = \frac{p_+ p_- p_{3c}}{(m_i^*)^3 T^3} \quad (4.37)$$

$$= \frac{(m_i^*)^{1/2} T^{13/2}}{2^{7/2} \pi^7} \int du_+ du_- du_{3c} d\gamma d\gamma_{3c} \sqrt{u_- - u_{3c}} (u_- - u_{3c})^2 \quad (4.38)$$

Using the center of mass momentum and simplifying the  $f_1 f_2 (1 - f_3) (1 - f_4)$  terms, the expression for the total rate integral becomes

$$\begin{aligned} \dot{\epsilon} = & \frac{S|\mathcal{M}|^2 (m_i^*)^{0.5} T^{6.5}}{2^{3.5} \pi^7} \int_0^\infty du_+ \int_0^\infty du_- \int_0^{u_-} du_{3c} \int_{-1}^1 d\gamma \int_{-1}^1 d\gamma_{3c} \sqrt{u_- - u_{3c}} \\ & \times (u_- - u_{3c})^2 f_1(u_1, y) f_2(u_2, y) [1 - f_3(u_3, y)] [1 - f_4(u_4, y)] \end{aligned} \quad (4.39)$$

In Eq. 4.39, we define a new dimensional variable

$$y = \frac{\mu - m^*}{T}. \quad (4.40)$$

This  $y$ -value included the chemical potential and effective mass of the particles in the medium. This can simplify the distribution such that

$$f = (e^{(E-\mu)/T} + 1)^{-1} \quad (4.41)$$

$$= (e^{(p^2/2m^* + m^* - \mu)/T} + 1)^{-1} \quad (4.42)$$

$$= (e^{u-y} + 1)^{-1} \quad (4.43)$$

The last variable substitution to simplify the integral (to reduce the computational complexity of the numerical integration) is to define

$$v = \frac{u_{3c}}{u_-} \quad \text{and} \quad q_{\pm} = e^{-u_{\pm}}, \quad (4.44)$$

With some effort to simplify the  $f_1 f_2 (1 - f_3)(1 - f_4)$  terms, the final expression becomes a three dimension rate integral,

$$\begin{aligned} \dot{\epsilon} = & \frac{S|\mathcal{M}|^2(m_i^*)^{0.5}T^{6.5}}{2^{3.5}\pi^7} \int_0^1 dq_+ \int_0^1 dq_- \int_0^1 dv q_+ q_- [(e^{-2y} - q_+^2 q_-^2)(1 - e^{2y-2vu_- - 2u_+})]^{-1} \\ & u_+^{-1/2} u_-^3 (1-v)^2 \ln \left[ \frac{\cosh[(u_+^{1/2} + u_-^{1/2})^2/2 - y/2]}{\cosh[(u_+^{1/2} - u_-^{1/2})^2/2 - y/2]} \right] \ln \left[ \frac{\cosh[((vu_-)^{1/2} + u_+^{1/2})^2/2 - y/2]}{\cosh[((vu_-)^{1/2} - u_+^{1/2})^2/2 - y/2]} \right] \end{aligned} \quad (4.45)$$

which matches the solution obtained by Brinkmann and Turner in ref. [44]. The matrix element from Eq. 2.18 can be approximated above  $T \geq 6$  MeV to be [44]

$$|\mathcal{M}|^2 = 256g_{ai}^2 f^4 m_i^2 / m_\pi^4. \quad (4.46)$$

There is no analytical solution to the emission rate integral, so numerical methods must be used. To relate the bremsstrahlung rate to the nucleon number density and temperature of the system, we must integrate the distribution function for the nucleons:

$$n_i = 2 \int_0^\infty \frac{d^3 p_i}{(2\pi)^3} f_i \quad \text{with } f_i = \frac{1}{e^{u_i - y_i} + 1} \quad (4.47)$$

$$= (\sqrt{2}/\pi^2)(m_i^* T)^{3/2} \int_0^\infty \frac{\sqrt{u_i} du_i}{e^{u_i - y_i} + 1} \quad \text{let } x = e^{-u_i} \quad (4.48)$$

$$= (\sqrt{2}/\pi^2)(m_i^* T)^{3/2} \int_0^1 \frac{dx}{x} \frac{\sqrt{-\ln(x)}}{e^{-y_i}/x + 1} \quad (4.49)$$

$$= (\sqrt{2}/\pi^2)(m_i^* T)^{3/2} I(y_i) \quad (4.50)$$

The density  $n_i$  is for either neutron density  $n_n$  or proton density  $n_p$ . A root solver can be used to get the  $y$ -value for either a medium full of neutrons  $y_n$  or protons  $y_p$ . Therefore,

the emission rate can be calculated at specific temperatures, varying densities, and effective masses.



## Part III

# RESULTS



## AXION BREMSSTRAHLUNG EMISSIVITIES

---

Axion emission rates inside a neutron star are primarily calculated through the nucleon-nucleon-axion bremsstrahlung mechanism, which can hypothetically be used to cool the neutron star. The following results show the axion emissivities in a homogeneous nuclear medium without gravitational effects. By changing the thermodynamic conditions of the medium, the axion emissivity is affected due to its dependence on temperature and density. The neutrino bremsstrahlung emissivities are also highly dependent on the temperature and density of the nuclear medium. This section is used to see the equation of state dependence of axion and neutrino emissivities and to compare axion and neutrino emissivities.

Testing the numerical calculations used (see Appendix A) to calculate Eq. 4.45 and compare to analytical approximations is done in Fig. 5.1. For this thesis, for the sake of estimation, we will only consider a nuclear medium of the same species: either all neutrons or all protons. Analytical approximations for the nondegenerate (ND) axion emission rates come from [43] [73]. From refs. [43] [73], the ND approximations are for the regions where  $y \ll -1$ , and assuming there is no Pauli blocking, so that the  $(1 - f_3)$  and  $(1 - f_4)$  terms are ignored, and also assuming the Fermi-Dirac distributions can be approximated to the Maxwell-Boltzmann distribution,

$$f \approx e^{[(E-\mu)/T]} \approx e^{u-y}. \quad (5.1)$$

Then, the simplification of the rate integral from Eq. 4.39 is

$$\dot{\epsilon}_a(\text{ND}) = \frac{1}{140\pi^{6.5}} S |\mathcal{M}|^2 m^{0.5} T^{6.5} e^{2y} \quad (5.2)$$

$$= 2.68 \times 10^{-4} e^{2y} m^{2.5} T^{6.5} m_\pi^{-4} g_{ai}^2 f^4 \quad (5.3)$$

where the  $y$ -value behaviour is exponential because of the two Maxwell-Boltzmann distributions for the two initial nucleons. Additionally, for the degenerate (D) approximation taken from ref. [48], the emission rate for the region  $y \gg 1$  takes the form,

$$\dot{\epsilon}_a(\text{D}) = \frac{31 \sqrt{2}}{241920\pi} S |\mathcal{M}|^2 m^{0.5} T^{6.5} y^{1/2} \quad (5.4)$$

$$= 3.69 \times 10^{-3} y^{1/2} m^{2.5} T^{6.5} m_\pi^{-4} g_{ai}^2 f^4 \quad (5.5)$$

where step functions for the Fermi-Dirac distributions are used to simplify the integral from Eq. 4.39 for the degenerate case. The dimensions of the emissivities will be in  $E^5$  from the  $m^{2.5} T^{6.5} m_\pi^{-4} g_{ai}^2 f^4$  term. Fig. 5.1 shows that the numerical results agree with the analytical approximations taken from refs. [43] [73] when  $y \ll -1$  for the ND case, and also agree with ref. [48] when  $y \ll 4$  for the D case.

Fig. 5.1 shows the analytical calculations hold well in the ND and D approximations by manually plugging in  $y$ -values into the analytical equations and the numerical equation (the other terms such as the  $g_{ai}$  and mass are neglected for now). Between  $0 \leq y \leq 4$ , the analytical approximations to the axion emissivity seem to overshoot the numerical emissivity. However, for the rest of the results, we will be working with an equation of state that is highly degenerate, with the  $y$ -value ranging between 0 and 100, which is far in the degenerate regime. Therefore, our numerical axion emissivity agrees with the analytical approximation made by ref. [48].

From the equation of state used, FSUGold2 [65], the slope of symmetry energy from Eq. 3.23, is equal to  $L = 47$  MeV,  $L = 60$  MeV, and  $L = 80$  MeV. This affects the difference in masses for protons and neutrons in the system at certain densities. The values of  $L$  are

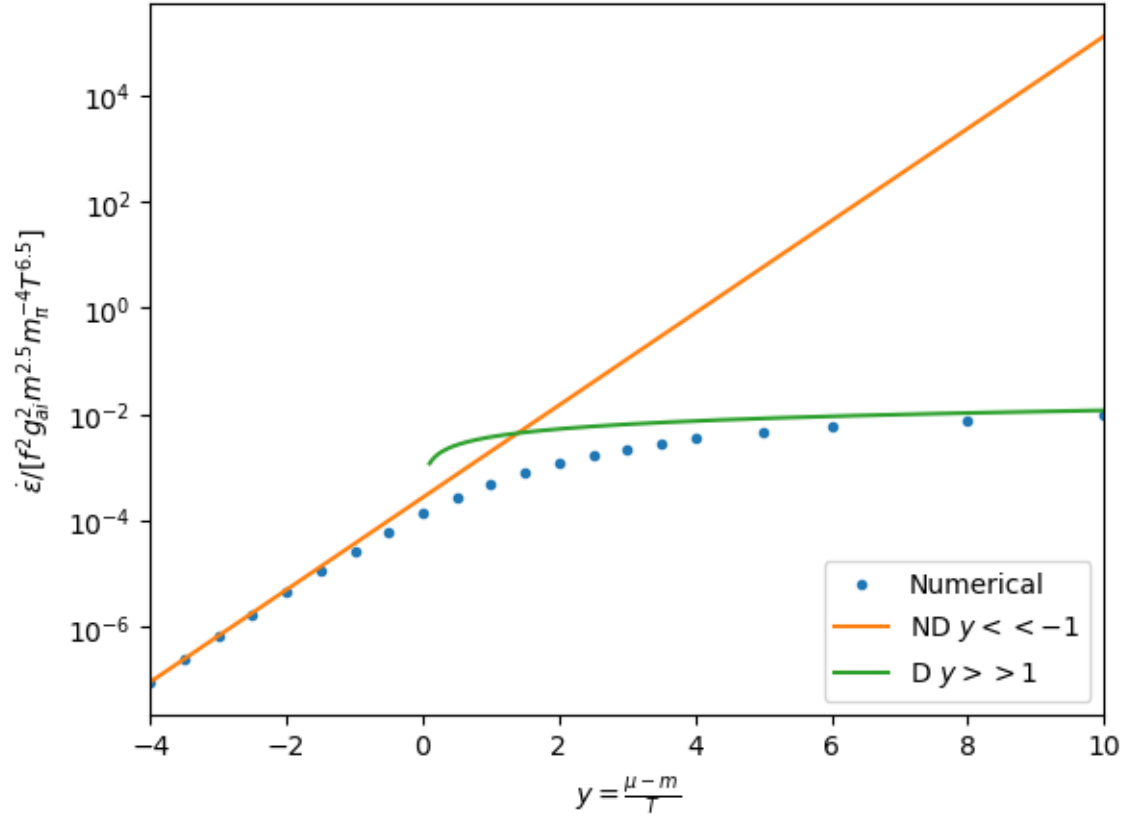


Figure 5.1: Analytical nucleon-nucleon-axion bremsstrahlung emission rates compared to numerical nucleon-nucleon-axion bremsstrahlung emission rates, within  $-4 \leq y \leq 10$  range. The results here are made dimensionless by only plotting the  $y$  dependent terms  $e^{2y}$  and  $y^{1/2}$ , and ignoring the  $f^2 g_{ai}^2 m^{2.5} m_\pi^{-4} T^{6.5}$  portion of the equations for the emissivities.

also chosen to span a range that is admissible to current neutron star studies [68]. For the FSUGold2 equation of state and for the results in this thesis, the nuclear saturation density is set to  $n_0 = 0.1504 \text{ fm}^{-3}$ .

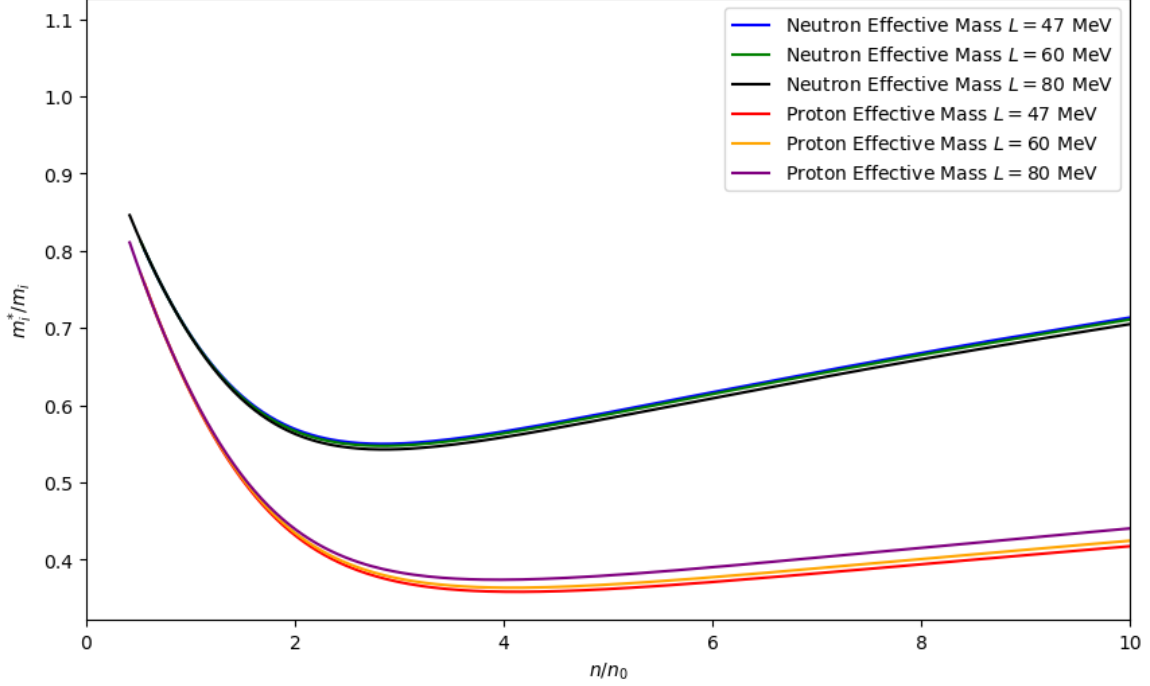


Figure 5.2: Ratio between effective mass and bare mass, which is  $m_p = 938\text{MeV}$  and  $m_n = 939\text{ MeV}$ , for proton and neutrons. The equation of state is FSUGold2 [65].

Fig. 5.2 shows the effective mass with  $L = 47\text{ MeV}$ ,  $L = 60\text{ MeV}$ , and  $L = 80\text{ MeV}$  at densities between  $0 < n/n_0 \leq 10$ . This density range is chosen since neutron star mergers can reach extreme densities several times larger than  $n_0$ . Therefore, in this study, the analysis will be up to  $10n_0$  to cover the density range for extreme nuclear conditions. We see that at all densities, the neutron effective mass is larger than the protons. At higher values of  $L$ , the neutron's effective mass is smaller in magnitude. For protons, the opposite effect is seen. Higher effective masses occur with higher values of  $L$ . By varying the  $L$  parameter, the EOS creates a bigger difference in effective masses between protons and neutrons.

Recall that the  $y$ -value is equal to,

$$y = \frac{\mu - m^*}{T}. \quad (5.6)$$

We can find the  $y$ -value by solving the expression from Eq. 4.50, by rearranging  $I(y_i)$  which is equal to,

$$I(y_i) = \int_0^1 \frac{dx}{x} \frac{\sqrt{-\ln(x)}}{e^{-y_i/x} + 1}, \quad (5.7)$$

and using a root solver to find the value of  $y_i$  at certain densities and effective masses since

$$I(y_i) = \frac{n}{(\sqrt{2}/\pi^2)(m^*T)^{3/2}}. \quad (5.8)$$

From Fig. 5.2, we see the effective masses decrease between  $0 < n/n_0 \leq 5$ , then increase, while in Fig. 5.3 the  $y$ -value behaviour is inverse; between  $0 < n/n_0 \leq 5$  the  $y$ -value increases, then decreases. This decrease in effective mass at lower densities is due to the large attractive contribution to the energy per nucleon, since there is a large condensed isoscalar-scalar  $\sigma$ -meson field [65]. As mass decreases within this region, the  $y$ -value increases, which is the respected behaviour since  $I(y_i) \propto e^y \propto (m^*)^{-3/2}$ . In Fig. 5.3, the temperature is set to  $T = 6$  MeV because our approximation for the matrix element used in Eq. 2.18 is valid for temperatures  $T \geq 6$  MeV [44].

For the axions emissivity, the results at  $T = 6$  MeV are shown in Fig. 5.4 and Fig. 5.5. These plots show a comparison with neutrino bremsstrahlung emissivities at the same temperature. The previous results from Fig. 5.1, Fig. 5.2, and Fig. 5.3 were not dependent on the coupling constant between nucleons and axions. For the rest of the results shown, we will be using the coupling constant given from [43],

$$g_{ai} = \frac{m_i^*}{2(f_a/N)} \quad (5.9)$$

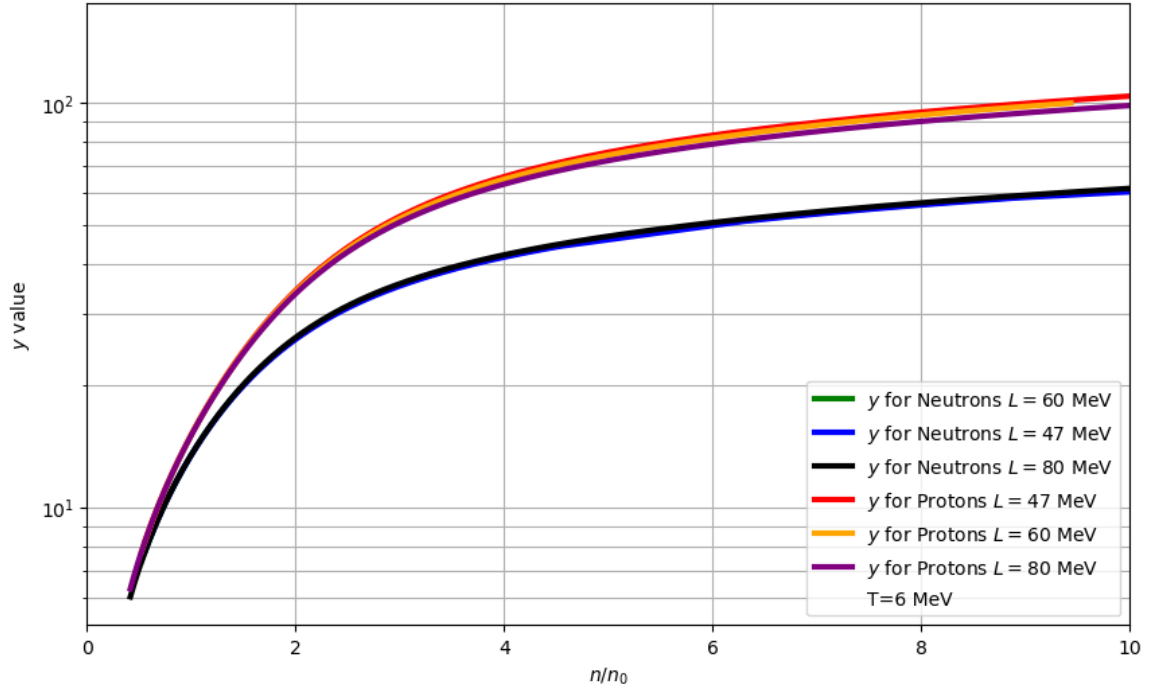


Figure 5.3: Shown is the  $y$ -value for neutrons and protons at increasing densities up to  $10n_0$ , where the temperature is set to  $T = 6$  MeV.

The coupling is proportional to the nucleon mass, adding an extra power of mass dependence to Eq. 4.45, giving the rates have the mass term have a power of  $m^{*1.5}$ . The following plots are taken for values of  $f_a/N = 8 \times 10^9$  GeV but from ref. [43], this can take values of  $f_a/N \geq 8 \times 10^9$  GeV,

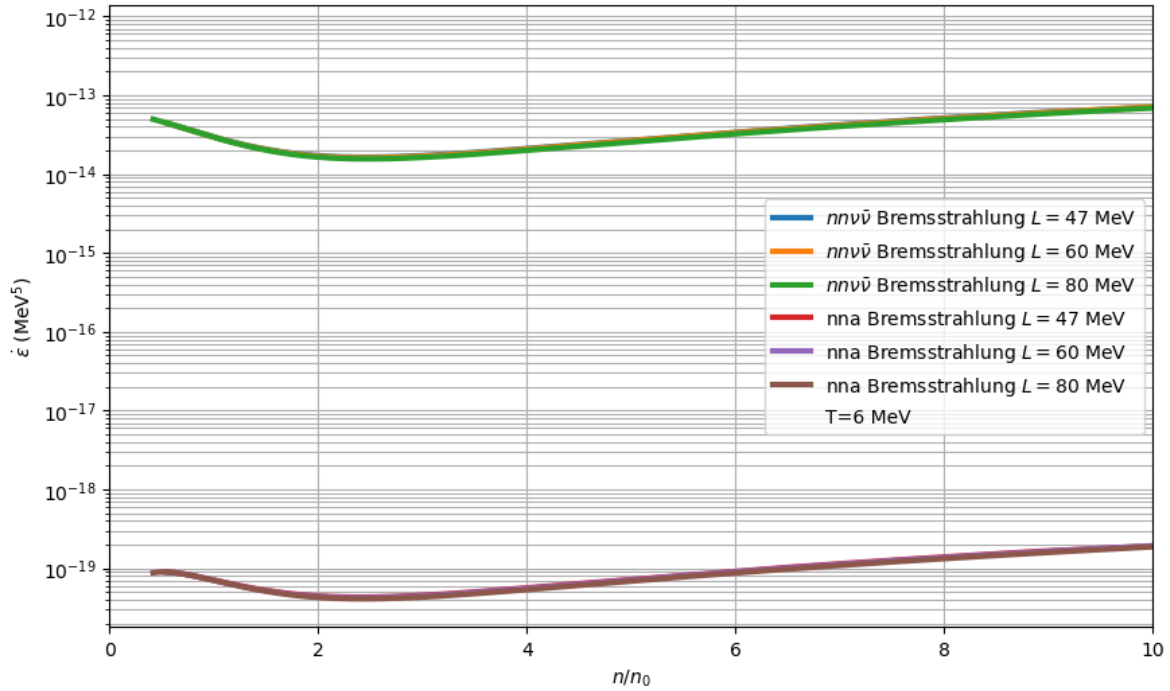


Figure 5.4: Neutron-neutron bremsstrahlung emission rates for axions and neutrinos at  $T = 6$  MeV.

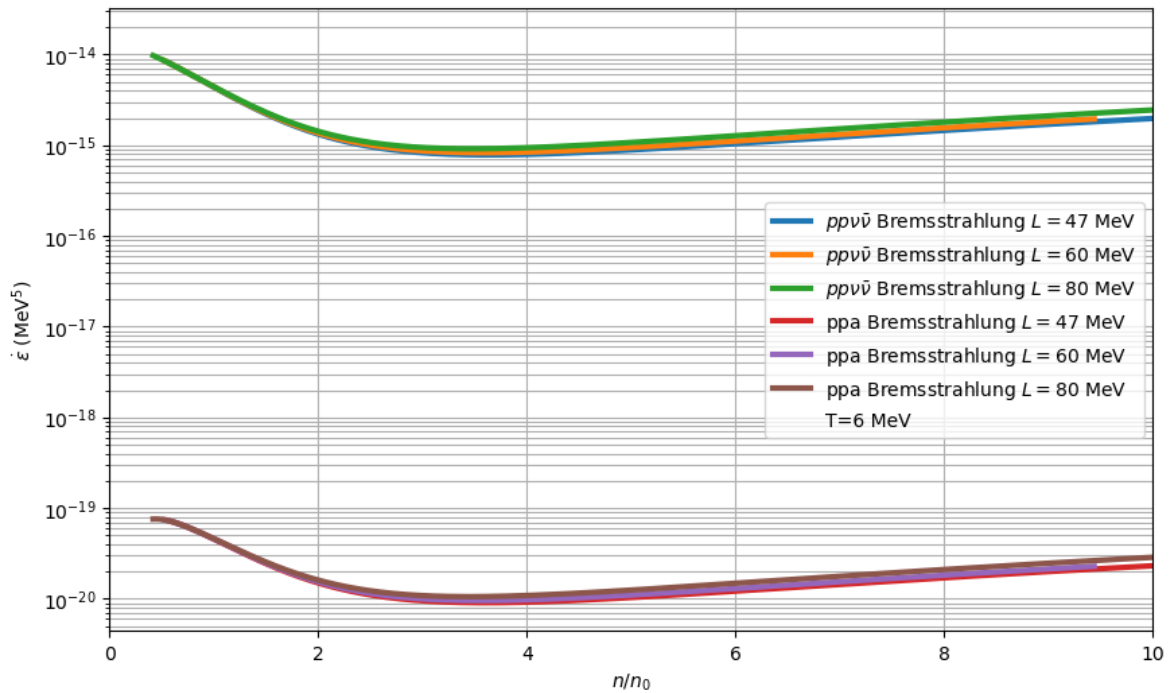


Figure 5.5: Proton-proton bremsstrahlung emission rates for axions and neutrinos at  $T = 6$  MeV.

Figs. 5.4 and 5.5 show the emission rates for neutron-neutron and proton-proton interactions, respectively, for the two types of bremsstrahlung processes. The difference in magnitude can be explained through the dependency on temperatures for the two different rates.

Seen from Eq. 4.45, Eq. 5.3, and Eq. 5.5, the power of temperature is  $T^{6.5}$ , which arises from the delta functions and Jacobian matrix when changing variables from momentum  $p$  to the dimensionless energy  $u = p^2/2mT$  for five particles. For neutrino rates, the power for temperature in Eq. 4.17 and Eq. 4.18 is  $T^8$ , which arises from the same process of changing variables from momentum  $p$  to the dimensionless energy  $x = p/T$  [57], but now for six particles in the interaction (four nucleons and two neutrinos) instead of five (four nucleons and one axion). Even though there are the same amount of nucleons in each process, the number of momentum terms accounts for the difference in the power of  $T$ . Therefore, the difference of one particle adds three more momentum terms in the phase space integral. The emission rates for neutron-neutron-axion bremsstrahlung and neutron-neutron-neutrino bremsstrahlung are about 10 times higher in magnitude compared to the proton-proton-axion bremsstrahlung and proton-proton-neutrino bremsstrahlung, respectively.

An interesting observation shown in Figs. 5.4 and 5.5 is that the  $L$  parameter does not affect the nucleon-nucleon-neutrino bremsstrahlung emission rates as much as nucleon-nucleon-axion bremsstrahlung. The different  $L$  parameters cause a larger difference in the proton-proton-axion bremsstrahlung compared with the neutron-neutron-axion bremsstrahlung. The higher the  $L$  parameter, the higher the proton-proton-axion bremsstrahlung emissivity. This difference is also seen in the proton effective mass in Fig. 5.2, where higher energy  $L$  causes the proton to gain more effective mass, which can impact the emissivities.

Increasing the temperature affects the overall rates due to the factor  $T^{6.5}$  for axion emission rates and  $T^8$  for neutrino emission rates. However, the axion rates are also affected by temperature when it comes to the  $y$ -value's dependence on temperature, which is proportional to  $T^{-1.5}$ . So, when temperature increases, the  $y$ -value magnitude decreases. This means the nuclear medium is getting less degenerate as temperature increases.

Fig. 5.6 shows the  $y$ -values at  $T = 10$  MeV, which is chosen to be used as a comparison to  $T = 6$  MeV. Compared to Fig. 5.3, which was as  $T = 6$  MeV, the  $y$ -values here are slightly less in magnitude. This trend continues at higher temperatures and is shown in Fig. 5.9.

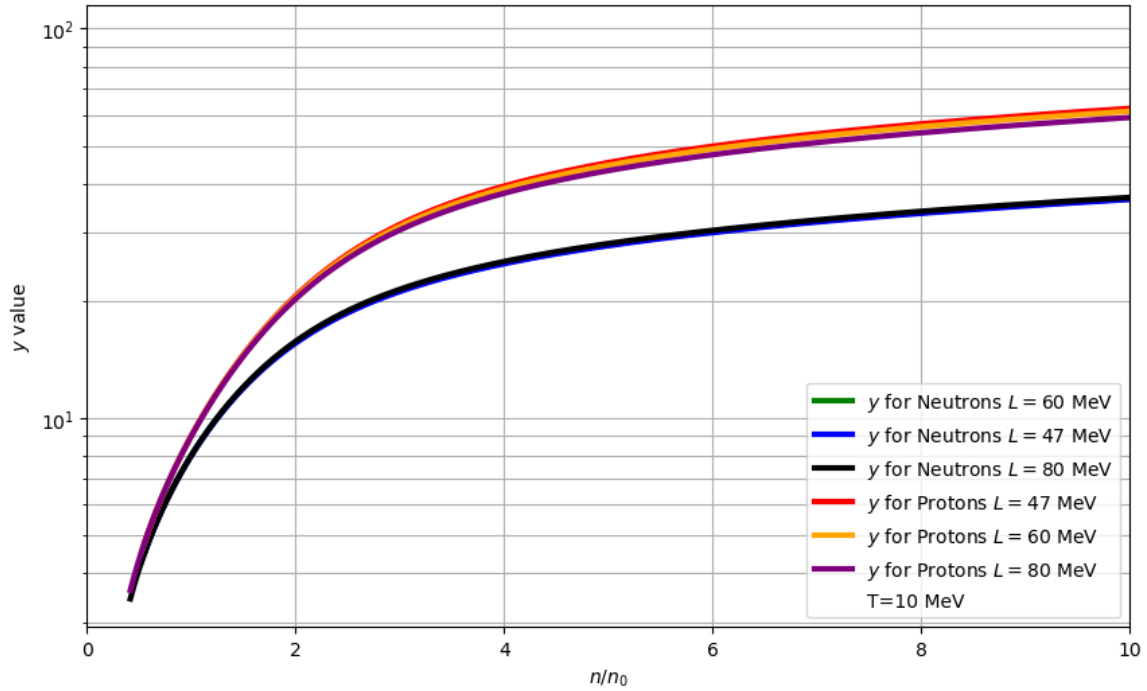


Figure 5.6: Shown is the  $y$ -value for neutrons and protons at increasing densities, with the temperature set to  $T = 10$  MeV.

By slightly increasing the temperature, the approximations for nucleon-nucleon-axion bremsstrahlung's emission rates become more accurate, as the approximation made for the matrix element  $|\mathcal{M}|^2$  was accurate for  $T \geq 6$  MeV [44].

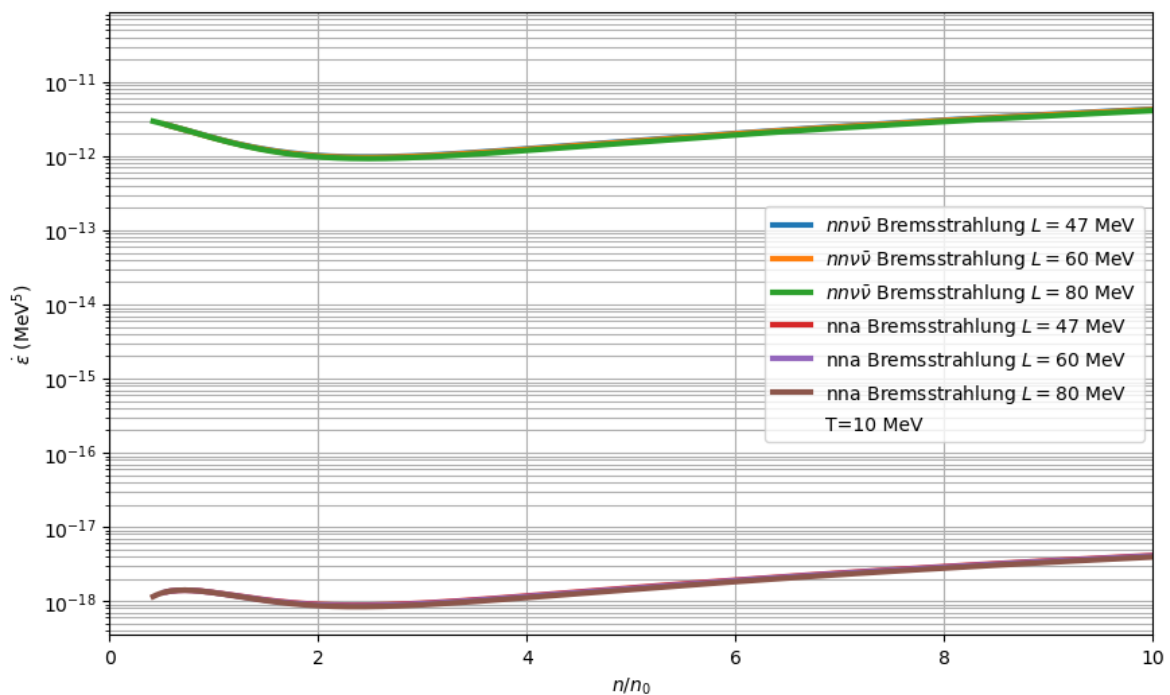


Figure 5.7: Neutron-neutron bremsstrahlung emission rates for axions and neutrinos at  $T = 10$  MeV.

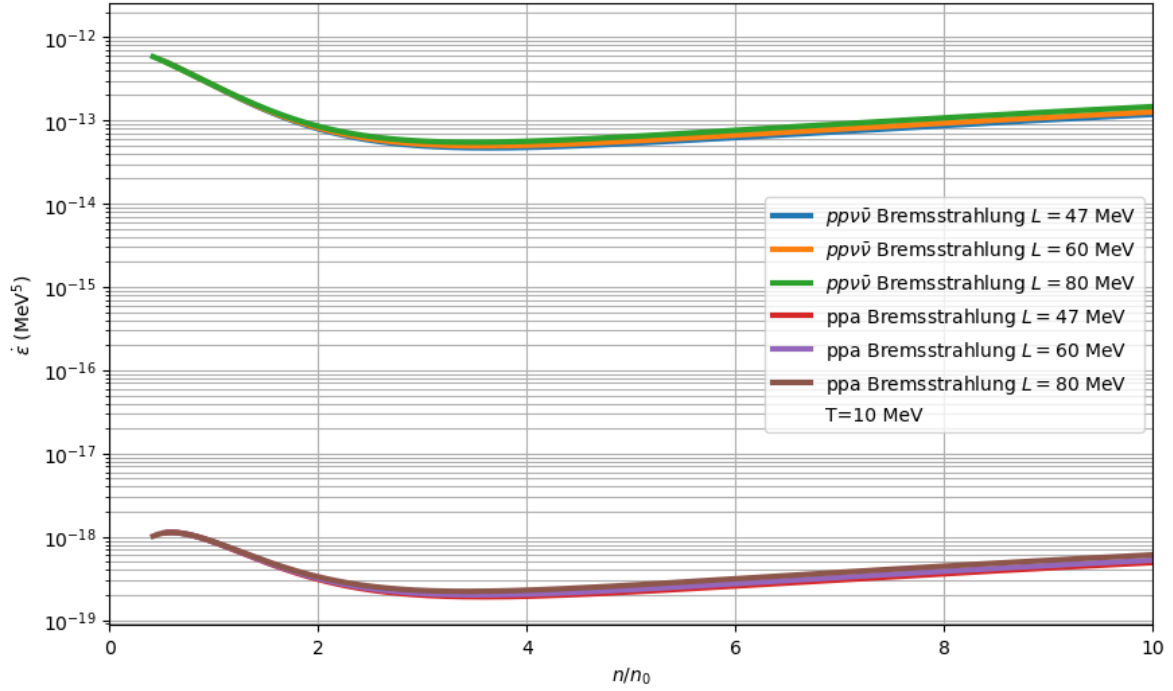


Figure 5.8: Proton-proton bremsstrahlung emission rates for axions and neutrinos at  $T = 10$  MeV.

Figs. 5.7 and 5.8 show the emission rates at  $T = 10$  MeV. At this temperature, the emission rates are higher compared to  $T = 6$  MeV. For temperatures well above this, the same temperatures seen in mergers (refer to section 3.0.2), the temperatures can reach up to  $T = 50$  MeV. For temperatures this high, the following results show the emissivities.

Fig. 5.9 shows the  $y$ -values at  $T = 50$  MeV for nuclear media.

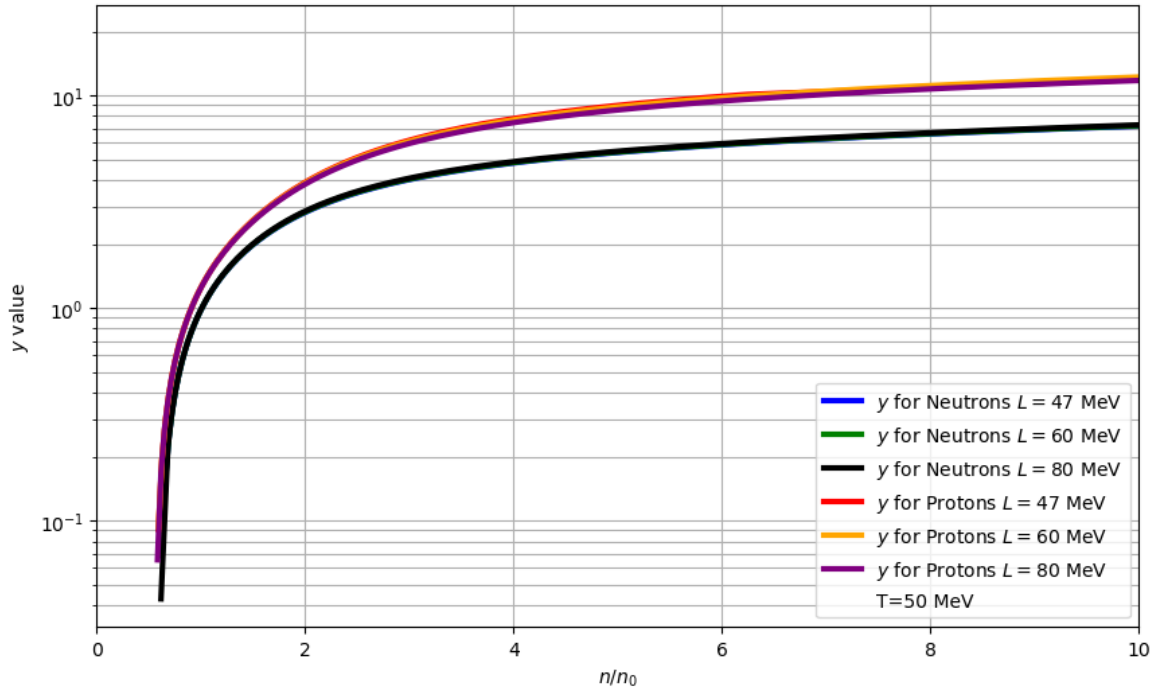


Figure 5.9: Shown is the y-value for neutrons and protons at increasing densities, for  $T = 50$  MeV.

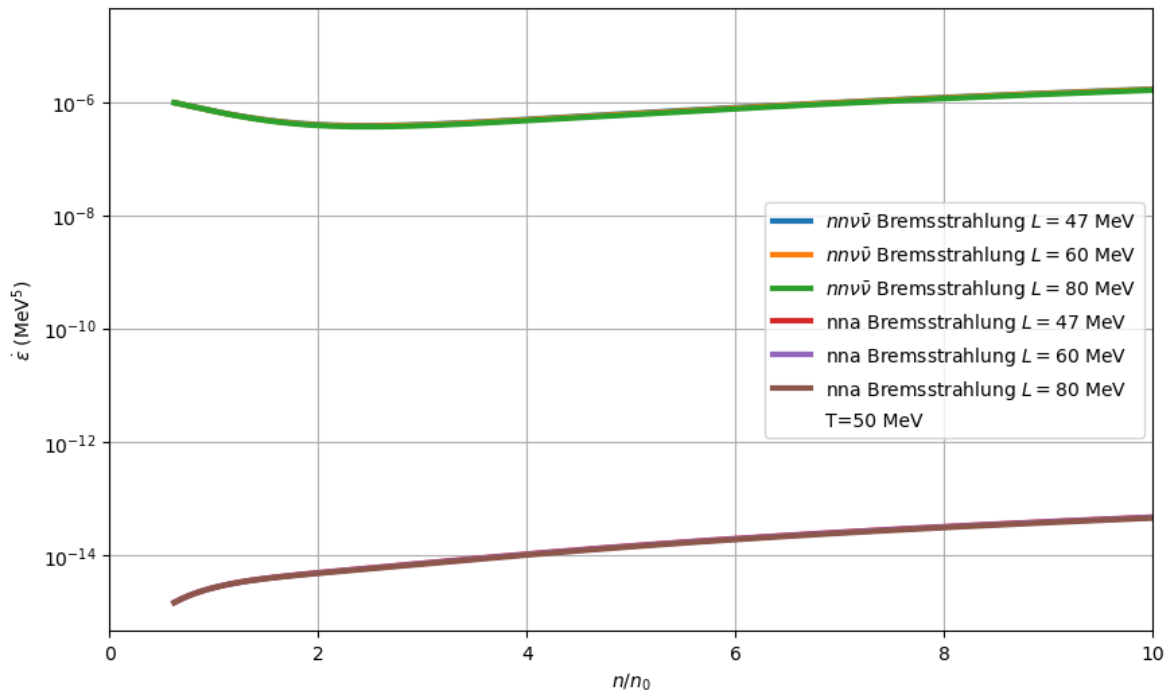


Figure 5.10: Neutron-neutron bremsstrahlung emission rates for axions and neutrinos at  $T = 50$  MeV.

Figs. 5.10 and 5.11 show the emission rates at  $T = 50$  MeV. It is interesting to note that the emission rates for the axion bremsstrahlung at this temperature match the same

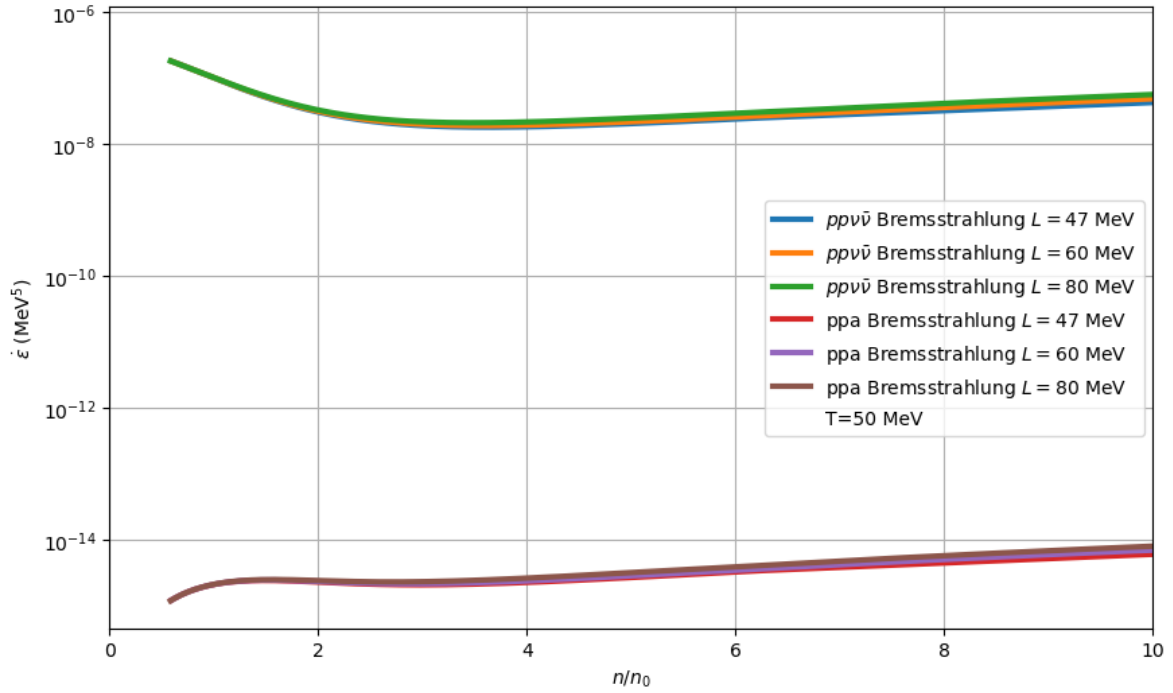


Figure 5.11: Proton-proton bremsstrahlung emission rates for axions and neutrinos at  $T = 50$  MeV.

magnitude that the neutrino bremsstrahlung reached at  $T = 6$  MeV, seen in Figs. 5.4 and 5.5.

## Part IV

# CONCLUSION



## CONCLUSION

---

In this thesis, the dynamics of axion emissions in extreme conditions in different regions of the QCD phase space are studied. These regions include nuclear matter at temperatures of  $T = 6$  MeV,  $T = 10$  MeV, and  $T = 50$  MeV for densities between  $0 < n/n_0 \leq 10$ . These temperatures were chosen since above  $T \geq 6$  MeV the approximations made for our axion bremsstrahlung matrix element hold,  $T = 10$  MeV is a still low temperature that can be used to compare the results for  $T = 6$  MeV, and  $T = 50$  MeV is chosen to see the effect of extremely high temperatures which are conditions that can be seen within neutron star mergers. The motivation for this work was to explore axion emissions under extreme conditions. The axion emissivities are compared to neutrino emissivity rates to quantify the magnitude difference between the two species. This included using equations of states that are highly baryon-dense. While Urca cooling processes have traditionally been considered the dominant cooling mechanism, exploring the circumstances under which axion emissions may equal or even surpass modified Urca cooling is interesting. In section 5, it is seen that neutron-neutron-neutrino bremsstrahlung and proton-proton-neutrino bremsstrahlung have a much higher emissivities compared to neutron-neutron-axion bremsstrahlung and proton-proton-axion bremsstrahlung. When the emissivities for neutron-neutron-axion bremsstrahlung and proton-proton-axion bremsstrahlung are compared, it is seen that neutron-neutron-axion bremsstrahlung is higher in magnitude. Lastly, it was shown that neutron-neutron-axion bremsstrahlung is not affected by the symmetry energy slope  $L$  as much as proton-proton-axion bremsstrahlung emission rates, where the difference between  $L = 47$  MeV,  $L = 60$  MeV, and  $L = 80$  MeV creates a notable change in the proton-proton-axion bremsstrahlung emissivities, where higher energy  $L$  increase the emissivities.

In all the results, there were no conditions found where axion bremsstrahlung emissivities surpassed neutrino bremsstrahlung emissivities.

This approach, mainly focusing on the impact of the symmetry energy slope  $L$  on axion emissivities under high-density conditions, extends the current understanding, especially given the increasing relevance of axion studies [74][75][76][77]. Further analysis of axion luminosity under extreme conditions may offer more insight. These studies could reveal distinct signatures of axion parameters, such as axion mass and nucleon-axion coupling. The inclusion of the axion may differ notably from neutrino-only models used to describe neutron star cooling [78], allowing phenomenological analysis utilizing temperature measurements obtained from satellite data. Future efforts will use the developed framework to study the equations of states near and at phase transitions in the QCD phase diagram and explore the different hypothetical crusts of neutron stars [79]. In future studies, solutions to the Tolman-Oppenheimer-Volkov (TOV) equations [80] in the neutron star models will also be considered.

Part V

APPENDIX

## C++ CODE

---

For the complete code used in this study, please refer to the GitHub repository at

[https://github.com/noahkakeka/axion\\_brem\\_rates/tree/main](https://github.com/noahkakeka/axion_brem_rates/tree/main)

## BIBLIOGRAPHY

---

- [1] Wikimedia Commons. *File:Standard Model of Elementary Particles.svg* — Wikimedia Commons, the free media repository. [Online; accessed 11-July-2024]. 2024. URL: [https://commons.wikimedia.org/w/index.php?title=File:Standard\\_Model\\_of\\_Elementary\\_Particles.svg&oldid=896377341](https://commons.wikimedia.org/w/index.php?title=File:Standard_Model_of_Elementary_Particles.svg&oldid=896377341).
- [2] R. L. Workman et al. “Review of Particle Physics.” In: *Progress of Theoretical and Experimental Physics* 2022 (2022), p. 083C01. doi: [10.1093/ptep/ptac097](https://doi.org/10.1093/ptep/ptac097).
- [3] J. G. de Swart, G. Bertone, and J. van Dongen. “How dark matter came to matter.” In: *Nature Astronomy* 1.3 (Mar. 2017). ISSN: 2397-3366. doi: [10.1038/s41550-017-0059](https://doi.org/10.1038/s41550-017-0059). URL: <http://dx.doi.org/10.1038/s41550-017-0059>.
- [4] S. M. Faber and J. S. Gallagher. “Masses and Mass-to-Light Ratios of Galaxies.” In: *Annual Review of Astronomy and Astrophysics* 17 (1979). Provided by the SAO/NASA Astrophysics Data System, pp. 135–187. doi: [10.1146/annurev.aa.17.090179.001031](https://doi.org/10.1146/annurev.aa.17.090179.001031). URL: <https://ui.adsabs.harvard.edu/abs/1979ARA&A..17..135F>.
- [5] D. P. Roy. *Basic Constituents of the Visible and Invisible Matter - A Microscopic View of the Universe*. 2000. arXiv: [physics/0007025](https://arxiv.org/abs/physics/0007025) [[physics.pop-ph](https://arxiv.org/abs/physics/0007025)].
- [6] Gerard Jungman, Marc Kamionkowski, and Kim Griest. “Supersymmetric dark matter.” In: *Physics Reports* 267.5 (1996), pp. 195–373. ISSN: 0370-1573. doi: [https://doi.org/10.1016/0370-1573\(95\)00058-5](https://doi.org/10.1016/0370-1573(95)00058-5). URL: <https://www.sciencedirect.com/science/article/pii/0370157395000585>.
- [7] Gianfranco Bertone and Dan Hooper. “History of dark matter.” In: *Reviews of Modern Physics* 90.4 (Oct. 2018). ISSN: 1539-0756. doi: [10.1103/revmodphys.90.045002](https://doi.org/10.1103/revmodphys.90.045002). URL: <http://dx.doi.org/10.1103/RevModPhys.90.045002>.

- [8] Daniel Abercrombie et al. “Dark Matter benchmark models for early LHC Run-2 Searches: Report of the ATLAS/CMS Dark Matter Forum.” In: *Physics of the Dark Universe* 27 (2020), p. 100371. ISSN: 2212-6864. DOI: <https://doi.org/10.1016/j.dark.2019.100371>. URL: <https://www.sciencedirect.com/science/article/pii/S2212686419301712>.
- [9] R. D. Peccei and Helen R. Quinn. “CP Conservation in the Presence of Pseudoparticles.” In: *Phys. Rev. Lett.* 38 (25 1977), pp. 1440–1443. DOI: [10.1103/PhysRevLett.38.1440](https://doi.org/10.1103/PhysRevLett.38.1440). URL: <https://link.aps.org/doi/10.1103/PhysRevLett.38.1440>.
- [10] Steven Weinberg. “A New Light Boson?” In: *Phys. Rev. Lett.* 40 (4 1978), pp. 223–226. DOI: [10.1103/PhysRevLett.40.223](https://doi.org/10.1103/PhysRevLett.40.223). URL: <https://link.aps.org/doi/10.1103/PhysRevLett.40.223>.
- [11] F. Wilczek. “Problem of Strong  $P$  and  $T$  Invariance in the Presence of Instantons.” In: *Phys. Rev. Lett.* 40 (5 1978), pp. 279–282. DOI: [10.1103/PhysRevLett.40.279](https://doi.org/10.1103/PhysRevLett.40.279). URL: <https://link.aps.org/doi/10.1103/PhysRevLett.40.279>.
- [12] Michael E. Peskin and Daniel V. Schroeder. *An Introduction to quantum field theory*. Reading, USA: Addison-Wesley, 1995. ISBN: 978-0-201-50397-5.
- [13] James M. Cline. *Advanced Concepts in Quantum Field Theory*. 2020. arXiv: [2005.10241](https://arxiv.org/abs/2005.10241) [hep-th].
- [14] Joseph I. Kapusta and Charles Gale. *Finite-Temperature Field Theory: Principles and Applications*. 2nd ed. Cambridge Monographs on Mathematical Physics. Cambridge University Press, 2006.
- [15] C. Drischler, J.W. Holt, and C. Wellenhofer. “Chiral Effective Field Theory and the High-Density Nuclear Equation of State.” In: *Annual Review of Nuclear and Particle Science* 71.1 (Sept. 2021), 403–432. ISSN: 1545-4134. DOI: [10.1146/annurev-nucl-102419-041903](https://doi.org/10.1146/annurev-nucl-102419-041903). URL: <http://dx.doi.org/10.1146/annurev-nucl-102419-041903>.

- [16] Larry McLerran and Robert D. Pisarski. “Phases of Dense Quarks at Large  $N_c$ .” In: *Nuclear Physics A* 796.1-4 (2007), pp. 83–100. ISSN: 0375-9474. DOI: [10.1016/j.nuclphysa.2007.08.013](https://doi.org/10.1016/j.nuclphysa.2007.08.013). URL: <http://dx.doi.org/10.1016/j.nuclphysa.2007.08.013>.
- [17] Larry McLerran. *Strongly Interacting Matter Matter at Very High Energy Density: 3 Lectures in Zakopane*. 2010. arXiv: [1011.3203](https://arxiv.org/abs/1011.3203) [hep-ph].
- [18] Mark Alford, Krishna Rajagopal, and Frank Wilczek. “QCD at finite baryon density: nucleon droplets and color superconductivity.” In: *Physics Letters B* 422.1-4 (Mar. 1998), 247–256. ISSN: 0370-2693. DOI: [10.1016/S0370-2693\(98\)00051-3](https://doi.org/10.1016/S0370-2693(98)00051-3). URL: [http://dx.doi.org/10.1016/S0370-2693\(98\)00051-3](http://dx.doi.org/10.1016/S0370-2693(98)00051-3).
- [19] Mark Alford, Krishna Rajagopal, and Frank Wilczek. “Color-flavor locking and chiral symmetry breaking in high density QCD.” In: *Nuclear Physics B* 537.1-3 (Jan. 1999), 443–458. ISSN: 0550-3213. DOI: [10.1016/S0550-3213\(98\)00668-3](https://doi.org/10.1016/S0550-3213(98)00668-3). URL: [http://dx.doi.org/10.1016/S0550-3213\(98\)00668-3](http://dx.doi.org/10.1016/S0550-3213(98)00668-3).
- [20] David J. Griffiths. *Introduction to Elementary Particles*. 2nd. Wiley-VCH, 2008. ISBN: 9783527406012.
- [21] Sidney Coleman. *Aspects of Symmetry: Selected Erice Lectures*. Cambridge University Press, 1985.
- [22] T. Schäfer and E. V. Shuryak. “Instantons in QCD.” In: *Reviews of Modern Physics* 70.2 (Apr. 1998), 323–425. ISSN: 1539-0756. DOI: [10.1103/revmodphys.70.323](https://doi.org/10.1103/revmodphys.70.323). URL: <http://dx.doi.org/10.1103/RevModPhys.70.323>.
- [23] Sidney R. Coleman. “The Uses of Instantons.” In: *Subnucl. Ser.* 15 (1979). Ed. by Mikhail A. Shifman, p. 805.
- [24] Maxim Pospelov and Adam Ritz. “Theta vacua, QCD sum rules, and the neutron electric dipole moment.” In: *Nuclear Physics B* 573.1-2 (May 2000), 177–200. ISSN: 0550-3213. DOI: [10.1016/S0550-3213\(99\)00817-2](https://doi.org/10.1016/S0550-3213(99)00817-2). URL: [http://dx.doi.org/10.1016/S0550-3213\(99\)00817-2](http://dx.doi.org/10.1016/S0550-3213(99)00817-2).

- [25] C. A. Baker et al. “Improved Experimental Limit on the Electric Dipole Moment of the Neutron.” In: *Physical Review Letters* 97.13 (Sept. 2006). ISSN: 1079-7114. DOI: [10.1103/PhysRevLett.97.131801](https://doi.org/10.1103/PhysRevLett.97.131801). URL: <http://dx.doi.org/10.1103/PhysRevLett.97.131801>.
- [26] R. D. Peccei and Helen R. Quinn. “Constraints Imposed by CP Conservation in the Presence of Instantons.” In: *Phys. Rev. D* 16 (1977), pp. 1791–1797. DOI: [10.1103/PhysRevD.16.1791](https://doi.org/10.1103/PhysRevD.16.1791).
- [27] Edward W. Kolb and Michael S. Turner. *The Early Universe*. Vol. 69. 1990. ISBN: 978-0-201-62674-2. DOI: [10.1201/9780429492860](https://doi.org/10.1201/9780429492860).
- [28] Szabolcs Borsanyi et al. “Calculation of the axion mass based on high-temperature lattice quantum chromodynamics.” In: *Nature* 539 (Nov. 2016), pp. 69–71. DOI: [10.1038/nature20115](https://doi.org/10.1038/nature20115).
- [29] P. Brun et al. “A new experimental approach to probe QCD axion dark matter in the mass range above 40  $\mu\text{eV}$ .” In: *The European Physical Journal C* 79.3 (Mar. 2019). ISSN: 1434-6052. DOI: [10.1140/epjc/s10052-019-6683-x](https://doi.org/10.1140/epjc/s10052-019-6683-x). URL: <http://dx.doi.org/10.1140/epjc/s10052-019-6683-x>.
- [30] Guy Moore. “Axion dark matter and the Lattice.” In: *EPJ Web of Conferences* 175 (2018). Ed. by M. Della Morte, P. Fritzsche, E. Gámiz Sánchez, and C. Pena Ruano, p. 01009. ISSN: 2100-014X. DOI: [10.1051/epjconf/201817501009](https://doi.org/10.1051/epjconf/201817501009). URL: <http://dx.doi.org/10.1051/epjconf/201817501009>.
- [31] Maria Paola Lombardo and Anton Trunin. “Topology and axions in QCD.” In: *International Journal of Modern Physics A* 35.20 (July 2020), p. 2030010. ISSN: 1793-656X. DOI: [10.1142/S0217751X20300100](https://doi.org/10.1142/S0217751X20300100). URL: <http://dx.doi.org/10.1142/S0217751X20300100>.
- [32] P. A. R. Ade et al. “Planck2015 results: XIII. Cosmological parameters.” In: *Astronomy and Astrophysics* 594 (Sept. 2016), A13. ISSN: 1432-0746. DOI: [10.1051/0004-6361/201525830](https://doi.org/10.1051/0004-6361/201525830). URL: <http://dx.doi.org/10.1051/0004-6361/201525830>.

- [33] David J.E. Marsh. “Axion cosmology.” In: *Physics Reports* 643 (July 2016), 1–79. ISSN: 0370-1573. DOI: [10.1016/j.physrep.2016.06.005](https://doi.org/10.1016/j.physrep.2016.06.005). URL: <http://dx.doi.org/10.1016/j.physrep.2016.06.005>.
- [34] N. Du et al. “Search for Invisible Axion Dark Matter with the Axion Dark Matter Experiment.” In: *Physical Review Letters* 120.15 (Apr. 2018). ISSN: 1079-7114. DOI: [10.1103/physrevlett.120.151301](https://doi.org/10.1103/physrevlett.120.151301). URL: <http://dx.doi.org/10.1103/PhysRevLett.120.151301>.
- [35] K. M. Backes et al. “A quantum enhanced search for dark matter axions.” In: *Nature* 590.7845 (Feb. 2021), 238–242. ISSN: 1476-4687. DOI: [10.1038/s41586-021-03226-7](https://doi.org/10.1038/s41586-021-03226-7). URL: <http://dx.doi.org/10.1038/s41586-021-03226-7>.
- [36] Sofia Kostoglou. “The CAST experiment at CERN.” MA thesis. Natl. Tech. U., Athens, June 2016.
- [37] E. Armengaud et al. “Physics potential of the International Axion Observatory (IAXO).” In: *Journal of Cosmology and Astroparticle Physics* 2019.06 (June 2019), 047–047. ISSN: 1475-7516. DOI: [10.1088/1475-7516/2019/06/047](https://doi.org/10.1088/1475-7516/2019/06/047). URL: <http://dx.doi.org/10.1088/1475-7516/2019/06/047>.
- [38] V.B. Bezerra, G.L. Klimchitskaya, V.M. Mostepanenko, and C. Romero. “Constraints on axion-nucleon coupling constants from measuring the Casimir force between corrugated surfaces.” In: *Physical Review D* 90.5 (Sept. 2014). ISSN: 1550-2368. DOI: [10.1103/physrevd.90.055013](https://doi.org/10.1103/physrevd.90.055013). URL: <http://dx.doi.org/10.1103/PhysRevD.90.055013>.
- [39] Luca Di Luzio et al. “Probing the axion–nucleon coupling with the next generation of axion helioscopes.” In: *The European Physical Journal C* 82.2 (Feb. 2022). ISSN: 1434-6052. DOI: [10.1140/epjc/s10052-022-10061-1](https://doi.org/10.1140/epjc/s10052-022-10061-1). URL: <http://dx.doi.org/10.1140/epjc/s10052-022-10061-1>.
- [40] Thomas Vonk, Feng-Kun Guo, and Ulf-G. Meißner. “Precision calculation of the axion-nucleon coupling in chiral perturbation theory.” In: *Journal of High Energy*

- Physics* 2020.3 (Mar. 2020). ISSN: 1029-8479. DOI: [10.1007/jhep03\(2020\)138](https://doi.org/10.1007/jhep03(2020)138).  
URL: [http://dx.doi.org/10.1007/JHEP03\(2020\)138](http://dx.doi.org/10.1007/JHEP03(2020)138).
- [41] Kim V. Berghaus, Matthew Forslund, and Mark Vincent Guevarra. “Minimal warm inflation with a heavy QCD axion.” In: (Feb. 2024). arXiv: [2402.13535](https://arxiv.org/abs/2402.13535) [hep-ph].
- [42] Ricardo Z. Ferreira, Alessio Notari, and Fabrizio Rompineve. “Dine-Fischler-Srednicki-Zhitnitsky axion in the CMB.” In: *Phys. Rev. D* 103 (6 2021), p. 063524. DOI: [10.1103/PhysRevD.103.063524](https://doi.org/10.1103/PhysRevD.103.063524). URL: <https://link.aps.org/doi/10.1103/PhysRevD.103.063524>.
- [43] Michael S. Turner. “Axions from SN1987A.” In: *Phys. Rev. Lett.* 60.18 (1988). Provided by the SAO/NASA Astrophysics Data System, pp. 1797–1800. DOI: [10.1103/PhysRevLett.60.1797](https://doi.org/10.1103/PhysRevLett.60.1797). URL: <https://ui.adsabs.harvard.edu/abs/1988PhRvL..60.1797T>.
- [44] Ralf Peter Brinkmann and Michael S. Turner. “Numerical rates for nucleon-nucleon, axion bremsstrahlung.” In: *Phys. Rev. D* 38 (8 1988), pp. 2338–2348. DOI: [10.1103/PhysRevD.38.2338](https://doi.org/10.1103/PhysRevD.38.2338). URL: <https://link.aps.org/doi/10.1103/PhysRevD.38.2338>.
- [45] David B. Kaplan. “Opening the Axion Window.” In: *Nucl. Phys. B* 260 (1985), pp. 215–226. DOI: [10.1016/0550-3213\(85\)90319-0](https://doi.org/10.1016/0550-3213(85)90319-0).
- [46] Mark Srednicki. “Axion couplings to matter: (I). CP-conserving parts.” In: *Nuclear Physics B* 260.3 (1985), pp. 689–700. ISSN: 0550-3213. DOI: [https://doi.org/10.1016/0550-3213\(85\)90054-9](https://doi.org/10.1016/0550-3213(85)90054-9). URL: <https://www.sciencedirect.com/science/article/pii/0550321385900549>.
- [47] Torleif Erik Oskar Ericson and W. Weise. *Pions and Nuclei*. Oxford, UK: Clarendon Press, 1988. ISBN: 978-0-19-852008-5.
- [48] Naoki Iwamoto. “Axion Emission From Neutron Stars.” In: *Phys. Rev. Lett.* 53 (12 1984), pp. 1198–1201. DOI: [10.1103/PhysRevLett.53.1198](https://doi.org/10.1103/PhysRevLett.53.1198). URL: <https://link.aps.org/doi/10.1103/PhysRevLett.53.1198>.

- [49] David Arnett and Roger Chevalier. “Supernovae and Nucleosynthesis: An Investigation of the History of Matter, from the Big Bang to the Present.” In: *Physics Today - PHYS TODAY* 49 (Oct. 1996). DOI: [10.1063/1.2807808](https://doi.org/10.1063/1.2807808).
- [50] S L Shapiro and S A Teukolsky. *Black holes, white dwarfs and neutron stars: The physics of compact objects*. Wiley, 1983. URL: <https://www.osti.gov/biblio/5869887>.
- [51] Jürgen Schaffner-Bielich. *Compact Star Physics*. Cambridge University Press, 2020.
- [52] C. J. Horowitz, J. Piekarewicz, and Brendan Reed. “Insights into nuclear saturation density from parity-violating electron scattering.” In: *Physical Review C* 102.4 (Oct. 2020). ISSN: 2469-9993. DOI: [10.1103/physrevc.102.044321](https://doi.org/10.1103/physrevc.102.044321). URL: <http://dx.doi.org/10.1103/PhysRevC.102.044321>.
- [53] M.E. Caplan and C.J. Horowitz. “Colloquium: Astromaterial science and nuclear pasta.” In: *Reviews of Modern Physics* 89.4 (Oct. 2017). ISSN: 1539-0756. DOI: [10.1103/revmodphys.89.041002](https://doi.org/10.1103/revmodphys.89.041002). URL: <http://dx.doi.org/10.1103/RevModPhys.89.041002>.
- [54] Dmitrii G Yakovlev, Kseniya P Levenfish, and Yurii A Shibarov. “Cooling of neutron stars and superfluidity in their cores.” In: *Physics-Uspekhi* 42.8 (Aug. 1999), 737–778. ISSN: 1468-4780. DOI: [10.1070/pu1999v042n08abeh000556](https://doi.org/10.1070/pu1999v042n08abeh000556). URL: <http://dx.doi.org/10.1070/PU1999v042n08ABEH000556>.
- [55] P. Haensel, A. Y. Potekhin, and D. G. Yakovlev. *Neutron stars 1: Equation of state and structure*. Vol. 326. New York, USA: Springer, 2007. DOI: [10.1007/978-0-387-47301-7](https://doi.org/10.1007/978-0-387-47301-7).
- [56] Eemeli Annala, Tyler Gorda, Alekski Kurkela, Joonas Nättilä, and Alekski Vuorinen. “Evidence for quark-matter cores in massive neutron stars.” In: *Nature Physics* 16.9 (June 2020), 907–910. ISSN: 1745-2481. DOI: [10.1038/s41567-020-0914-9](https://doi.org/10.1038/s41567-020-0914-9). URL: <http://dx.doi.org/10.1038/s41567-020-0914-9>.

- [57] D Yakovlev. “Neutrino emission from neutron stars.” In: *Physics Reports* 354.1–2 (Nov. 2001), 1–155. ISSN: 0370-1573. DOI: [10.1016/S0370-1573\(00\)00131-9](https://doi.org/10.1016/S0370-1573(00)00131-9). URL: [http://dx.doi.org/10.1016/S0370-1573\(00\)00131-9](http://dx.doi.org/10.1016/S0370-1573(00)00131-9).
- [58] Hao Tong and Qiu-He Peng. “Improbability of DUrca Process Constraints EOS.” In: *Chinese Journal of Astronomy and Astrophysics* 7.6 (Dec. 2007), 809–813. ISSN: 1009-9271. DOI: [10.1088/1009-9271/7/6/08](https://doi.org/10.1088/1009-9271/7/6/08). URL: <http://dx.doi.org/10.1088/1009-9271/7/6/08>.
- [59] Keisuke Yanagi. *Thermal Evolution of Neutron Stars as a Probe of Physics beyond the Standard Model*. 2020. arXiv: [2003.08199](https://arxiv.org/abs/2003.08199) [hep-ph].
- [60] G. G. Raffelt. *Stars as Laboratories for Fundamental Physics: The Astrophysics of Neutrinos, Axions, and Other Weakly Interacting Particles*. University of Chicago Press, 1996. ISBN: 978-0-226-70272-8. DOI: [10.7208/chicago/9780226702735.001.0001](https://doi.org/10.7208/chicago/9780226702735.001.0001).
- [61] Caiwan Shen, U. Lombardo, N. Van Giai, and W. Zuo. “Neutrino mean free path in neutron stars.” In: *Physical Review C* 68.5 (Nov. 2003). ISSN: 1089-490X. DOI: [10.1103/physrevc.68.055802](https://doi.org/10.1103/physrevc.68.055802). URL: <http://dx.doi.org/10.1103/PhysRevC.68.055802>.
- [62] M. Oertel, M. Hempel, T. Klähn, and S. Typel. “Equations of state for supernovae and compact stars.” In: *Reviews of Modern Physics* 89.1 (Mar. 2017). ISSN: 1539-0756. DOI: [10.1103/revmodphys.89.015007](https://doi.org/10.1103/revmodphys.89.015007). URL: <http://dx.doi.org/10.1103/RevModPhys.89.015007>.
- [63] Bryce Fore and Sanjay Reddy. “Pions in hot dense matter and their astrophysical implications.” In: *Physical Review C* 101.3 (Mar. 2020). ISSN: 2469-9993. DOI: [10.1103/physrevc.101.035809](https://doi.org/10.1103/physrevc.101.035809). URL: <http://dx.doi.org/10.1103/PhysRevC.101.035809>.

- [64] Miriam Hein, Alexander Pusch, and Stefan Heusler. “Modeling in nuclear physics: a visual approach to the limitations of the semi-empirical mass formula.” In: *Eur. J. Phys.* 43.3 (2022), p. 035801. DOI: [10.1088/1361-6404/ac4d7c](https://doi.org/10.1088/1361-6404/ac4d7c).
- [65] F. Fattoyev. “Sensitivity of Neutron Star Properties to the Equation of State.” PhD thesis. Florida State University, 2011. URL: [http://purl.flvc.org/fsu/fd/FSU\\_migr\\_etd-4824](http://purl.flvc.org/fsu/fd/FSU_migr_etd-4824).
- [66] LieWen Chen. “Higher order bulk characteristic parameters of asymmetric nuclear matter.” In: *Science China Physics, Mechanics and Astronomy* 54.S1 (July 2011), 124–129. ISSN: 1869-1927. DOI: [10.1007/s11433-011-4415-9](https://doi.org/10.1007/s11433-011-4415-9). URL: <http://dx.doi.org/10.1007/s11433-011-4415-9>.
- [67] J. Piekarewicz and M. Centelles. “Incompressibility of neutron-rich matter.” In: *Phys. Rev. C* 79 (5 2009), p. 054311. DOI: [10.1103/PhysRevC.79.054311](https://doi.org/10.1103/PhysRevC.79.054311). URL: <https://link.aps.org/doi/10.1103/PhysRevC.79.054311>.
- [68] Melissa Mendes Silva. “Nuclear equations of state, superfluidity models and cold neutron star observations.” PhD thesis. McGill University, 2023.
- [69] Wei-Chia Chen and J. Piekarewicz. “Building relativistic mean field models for finite nuclei and neutron stars.” In: *Phys. Rev. C* 90 (4 2014), p. 044305. DOI: [10.1103/PhysRevC.90.044305](https://doi.org/10.1103/PhysRevC.90.044305). URL: <https://link.aps.org/doi/10.1103/PhysRevC.90.044305>.
- [70] Mirco Cannoni. “Lorentz invariant relative velocity and relativistic binary collisions.” In: *International Journal of Modern Physics A* 32.02n03 (Jan. 2017), p. 1730002. ISSN: 1793-656X. DOI: [10.1142/S0217751X17300022](https://doi.org/10.1142/S0217751X17300022). URL: <http://dx.doi.org/10.1142/S0217751X17300022>.
- [71] Carlo Cercignani and Gilberto Medeiros Kremer. *The Relativistic Boltzmann Equation: Theory and Applications*. Birkhäuser, 2002. URL: <https://ui.adsabs.harvard.edu/abs/2002rbet.book.....C>.

- [72] D. H. Wilkinson. “Renormalization of the Axial-Vector Coupling Constant in Nuclear beta Decay.” In: *Phys. Rev. C* 7 (1973), pp. 930–936. doi: [10.1103/PhysRevC.7.930](https://doi.org/10.1103/PhysRevC.7.930).
- [73] Ron Mayle, James R. Wilson, John Ellis, Keith Olive, David N. Schramm, and Gary Steigman. “Constraints on axions from SN 1987A.” In: *Physics Letters B* 203.1 (1988), pp. 188–196. ISSN: 0370-2693. doi: [https://doi.org/10.1016/0370-2693\(88\)91595-X](https://doi.org/10.1016/0370-2693(88)91595-X). URL: <https://www.sciencedirect.com/science/article/pii/037026938891595X>.
- [74] Tobias Fischer, Pierluca Carenza, Bryce Fore, Maurizio Giannotti, Alessandro Mirizzi, and Sanjay Reddy. “Observable signatures of enhanced axion emission from protoneutron stars.” In: *Physical Review D* 104.10 (Nov. 2021). ISSN: 2470-0029. doi: [10.1103/PhysRevD.104.103012](https://doi.org/10.1103/PhysRevD.104.103012). URL: <http://dx.doi.org/10.1103/PhysRevD.104.103012>.
- [75] Armen Sedrakian. “Axion cooling of neutron stars.” In: *Physical Review D* 93.6 (Mar. 2016). ISSN: 2470-0029. doi: [10.1103/PhysRevD.93.065044](https://doi.org/10.1103/PhysRevD.93.065044). URL: <http://dx.doi.org/10.1103/PhysRevD.93.065044>.
- [76] Avik Paul, Debasish Majumdar, and Kamakshya Prasad Modak. “Neutron star cooling via axion emission by nucleon–nucleon axion bremsstrahlung.” In: *Pramana* 92.3 (2019), p. 44. doi: [10.1007/s12043-018-1702-2](https://doi.org/10.1007/s12043-018-1702-2). arXiv: [1801.07928 \[hep-ph\]](https://arxiv.org/abs/1801.07928).
- [77] Tobias Fischer, Sovan Chakraborty, Maurizio Giannotti, Alessandro Mirizzi, Alexandre Payez, and Andreas Ringwald. “Probing axions with the neutrino signal from the next Galactic supernova.” In: *Physical Review D* 94.8 (Oct. 2016). ISSN: 2470-0029. doi: [10.1103/PhysRevD.94.085012](https://doi.org/10.1103/PhysRevD.94.085012). URL: <http://dx.doi.org/10.1103/PhysRevD.94.085012>.
- [78] A Y Potekhin, D A Zyuzin, D G Yakovlev, M V Beznogov, and Yu A Shibano. “Thermal luminosities of cooling neutron stars.” In: *Monthly Notices of the Royal*

- Astronomical Society* 496.4 (June 2020), 5052–5071. ISSN: 1365-2966. DOI: [10.1093/mnras/staa1871](https://doi.org/10.1093/mnras/staa1871). URL: <http://dx.doi.org/10.1093/mnras/staa1871>.
- [79] B. G. Todd-Rutel and J. Piekarewicz. “Neutron-Rich Nuclei and Neutron Stars: A New Accurately Calibrated Interaction for the Study of Neutron-Rich Matter.” In: *Phys. Rev. Lett.* 95 (12 2005), p. 122501. DOI: [10.1103/PhysRevLett.95.122501](https://doi.org/10.1103/PhysRevLett.95.122501). URL: <https://link.aps.org/doi/10.1103/PhysRevLett.95.122501>.
- [80] J. R. Oppenheimer and G. M. Volkoff. “On Massive Neutron Cores.” In: *Phys. Rev.* 55 (4 1939), pp. 374–381. DOI: [10.1103/PhysRev.55.374](https://doi.org/10.1103/PhysRev.55.374). URL: <https://link.aps.org/doi/10.1103/PhysRev.55.374>.